SSSU 88
ISSN 0140 3818

Approaches to Assessment of Damage Tolerance Levels in FRP Structures

H.J. Phillips and R.A. Shenoi

Ship Science Report Number 88

May 1995

SSSU 88
ISSN 0140 3818

UNIVERSITY OF SOUTHAMPTON

DEPARTMENT OF SHIP SCIENCE

FACULTY OF ENGINEERING AND APPLIED SCIENCE

Approaches to Assessment of Damage Tolerance Levels in FRP Structures

H.J. Phillips and R.A. Shenoi

Ship Science Report Number 88

May 1995

APPROACHES TO ASSESSMENT OF DAMAGE TOLERANCE LEVELS IN FRP STRUCTURES

by

H. J. PHILLIPS

R. A. SHENOI

UNIVERSITY OF SOUTHAMPTON

DEPARTMENT OF SHIP SCIENCE

MAY 1995

CONTENTS

1. INTRODUCTION.

This report concerns damage tolerance levels in FRP ships and is a follow-on to two previous University of Southampton reports [1,2]. The principal damage scenario concerns delaminations in plating and in secondary bonds associated with T-joints (such as those between bulkhead and shell plating). The purpose of this report is to discuss three main topics related to compressive behaviour of delaminated beams, stress pattern modelling of T-joints and fracture criteria in assessment of joint adequacy.

The analytical and numerical FE modelling of delaminated beams has been covered before [2]. It was shown that a closed form analytical solution can give a good estimate of the critical buckling load in comparison with experimental results [3]. Some discrepencies were however noted in the FE model results. This report outlines an alternative approach which overcomesthe problems associated with the previous model and presents new results which tally with the experimental and analytical values.

T-joints represent a potential area of structural weakness in all FRP ships and it is therefore important to understand the load transfers and failure mechanisms associated with them. Experimental work has been carried out at DRA characterising load-deflection behaviour coupled with visual observations of failure [4]. This report presents the results of an FE model of the test configuration and hence the causes of failure.

Finally, because the failure pattern (owing to delamination) represents in-plane cracks, an attempt has been made to introduce fracture mechanics criteria in evaluating T-joint performance. This preliminary effort has been targetted to determining J-integral values for a T-joint with isotropic material.

2. THEORETICAL MODELLING OF DELAMINATED BEAM SPECIMENS

2.1. BACKGROUND.

An attempt was made to model the compression tests [3] carried out at Dunfermline on delaminated beam specimens. Both analytical formulation and finite element methods were used for the modelling.

2.2. EXPERIMENTATION.

Compression tests were carried out on two types of specimens:

(a) Hand-lay up specimens

(b) Vacuum assisted Resin Transfer (V.R.T.) specimens

For each type, the delamination was located at different depths below the outer surface. In addition, the delamination length was varied.

The nominal thickness of the hand lay-up specimens was 20 mm and that of the V.R.T. specimens was 12.7 mm. In all cases, the beam length between grips was 240 mm and the width was 50 mm. The delamination depths were varied as shown in table 2.1.

For each test, the stress at which the beam buckled was calculated. It is these values of critical buckling stress which have been calculated using analytical and numerical techniques.

2.3. MODELLING TECHNIQUES.

2.3.1. Analytical formulation.

This technique was presented in a previous report [1]. For a delaminated beam loaded in compression, as shown in figure 2.1, the critical stress at which it will buckle can be yielded from the equation 1.

$$\frac{\lambda_1 t_1^3}{6\sin\lambda_1 l_1}\cos\lambda_1 l_1 + \frac{\lambda_1 t_2^2 t_1}{6\sin\frac{\lambda_1 l_2 t_1}{2t_2}}\cos\frac{\lambda_1 t_1 l_2}{2t_2} + \frac{\lambda_1 t_3^2 t_1}{6\sin\frac{\lambda_1 l_3 t_1}{2t_3}}\cos\frac{\lambda_1 l_3 t_1}{2t_3}$$

$$+ \frac{t_1 t_2 t_3}{l_3} = 0 \qquad (1)$$

where: t_i is the thickness of part i (i=1,2,3).

l_i is the length of part i (i=1,2,3).

λ_1 is given below when i=1.

$$\lambda_i^2 = \frac{P_i}{D_i^*} \quad ; \quad D_i^* = \frac{E t_i^3}{12(1-\nu^2)} \qquad (2)$$

and P_i is the axial force per unit length in the i^{th} part.

D_i^* is the stiffness of the i^{th} part.

t_i is the thickness of the i^{th} part.

E is the Young's modulus.

ν is the Poisson ratio.

For a given beam specimen, the values of t and l are known and can be entered into equation (1). The equation can then be solved to yield a the lowest value of λ_1 for which the equation is satisfied. The value of P_1 can then be calculated from equation 2 and hence the critical buckling stress for the beam is obtained. The results of the experiments are compared with this

analysis and are shown in figures 2.2(a)-2.2(e) for the hand lay-up specimens and in figures 2.3(a)-2.3(d) for the V.R.T. specimens. For the hand lay-up specimens, when the depth of the in-built delamination is 0.8 mm below the outer surface (T3 = 0.8 mm), it can be seen that the analytical model gives results which are above the experimental values. When the depth of the delamination increases to 1.7 mm, 2.5 mm, 3.3 mm and 4.2 mm it is noted that the analytical model gives results which gradually fall below the experimental data points. For the V.R.T. specimens, the analytical points lie, in general, above the experimental data points.

2.3.2. Finite Element Modelling.

The results of the 3D analysis discussed in the previous report [2] gave adequate results when compared with the experimental and analytical results. However, meshing problems were encountered. The number of elements along the defect region effected both the critical buckling stress as well as the buckled shape. The defect region is shown in figure 2.4. An example of the results obtained from the previous modelling technique is given in table 2.2.

It can be seen that as the number of elements along the defect region increases, the values for the critical buckling stress decrease. However, there is a critical point at which the buckled shape becomes non-typical. Examples of typical and non-typical buckled shapes are shown in figures 2.5(a) and 2.5(b) respectively. It became evident that this type of meshing technique was inadequate.

In order to overcome this problem the following changes were made to the model:

(A) The beam was modelled in only two dimensions i.e length and thickness. Since the experimental beam width (50 mm) is of the same order of dimension as the beam length (240 mm) and thickness (20 mm for the hand lay-up specimens and 12.7 mm for the V.R.T. specimens) conditions of plane stress were assumed to exist.

(B) A technique of automatic meshing was adopted with, in this case, 2D plane stress elements. An example of such a model is given in figure 2.6.

2.4. FINAL RESULTS.

A sample of the results using the changed finite element model has produced improved results, see table 2.3. The critical buckling stress values are achieved from only one analysis. In addition, the buckled shape of the beams is that of the typical mode. The 2D results for one case also compare favourably with the equivalent 3D result.

2.5. CONCLUSIONS.

The two dimensional plane stress finite element analysis has provided a consistent method of calculating the critical buckling stress of compressively loaded delaminated beams. The results also compare well with both the experimental values and those obtained from analytical formulations.

3. T-JOINT BEHAVIOUR

3.1 BACKGROUND.

Static three-point bending tests were carried out on T-joint specimens [4]. Load and deflection were measured using a calibrated load cell and transducer respectively. A diagram of the load set-up is shown in figure 3.1. The material used in the T-joints and the lay-up arrangements in the overlaminate, web and flange are shown in figure 3.2.

A series of finite element models were generated with a view to understand internal load transfer mechanisms. The stress patterns associated with the load transfer were obtained for key load levels where noticeable damage occurred in the experiments. The key load levels are discussed in detail in the following paragraphs.

The finite element models were used to mirror the experimental load-deflection curve. Descriptions of the experimental failure patterns are given in table 3.1 and are shown graphically in figure 3.3.

It can be noted that changes in slope of the load-deflection curve occur at loads of 5500 N, 7500 N, 8600 N, 11500 N, 13000 N, 17600 N and 19000 N when the specimen finally failed. These changes of slope may be accounted for to a certain degree by the observations noted above.

3.2 FINITE ELEMENT MODELS.

3.2.1. Introduction.

Initially, a full 3D model was generated which yielded acceptable results for the initial stiffness of the undamaged model. In an attempt to reduce the complexity of the modelling, a 2D model was generated. The loading and geometry of the joints were symmetrical which made it possible to only model half the joint. So as to model the delaminations in the overlaminate which occurred in the tests, one element per layer was modelled. To represent the symmetry of the model, all the nodes along the centre-line of the web were allowed free movement in the loading direction (y-direction) but were restricted in the x-direction. The initial results for the undamaged model were compared with those generated from the full 3D model to verify that it was acceptable to proceed using only 2D models. The two sets of results were also compared with the experimental value of deflection at a load of 5500 N to check the accuracy of the finite element models. The results are given in table 3.2.

It was noted that during the experiments, the web was seen to bend over away from the damage zone. For this reason it was thought necessary to model the entire joint. A typical finite element model used in the analysis along with the coordinate system used is shown in figure 3.4.

3.2.2 Assumptions used.

The assumptions which were used whilst generating the models are given as follows:

(a) Plane strain conditions are assumed to prevail in the 2D models since the joint can be considered wide in relation to the length and thickness.

(b) For the 2D models, the finite element load applied is equal to the experimental load per unit width of joint.

(c) In the three-point bending experiments, the flange is supported by two rollers. These are represented in the finite element models by restricting the nodes at the two appropriate locations in the y direction, as shown in figure 3.4. In addition, in order to prevent rigid body motion, one of these nodes is also restricted in the x-direction.

(d) The damage zones (i.e the debond, fillet crack and delaminations) in the joints were modelled by inserting a small gap between the relevant elements.

(e) The material properties used in the analyses are given in table 3.3. It should be pointed out that due to the lay-up direction and the model coordinate system, the values given for Ex and Ey for Polyester/Woven Roving are E weft and Ez for the equivalent 3D model.

3.2.3 Modelling T-joint Experimental Damage.

A total of 6 models have been generated:

- MODEL 1 undamaged model
- MODEL 2 model representing damage type 'A' given in Table 3.1
- MODEL 3 model representing damage type 'B' given in Table 3.1
- MODEL 4 model representing damage type 'C' given in Table 3.1
- MODEL 5 model representing damage type 'D' given in Table 3.1
- MODEL 6 is the same as MODEL 5 with further delamination between the web/overlaminate and flange/overlaminate interfaces

All models utilised the non-linear geometry to account for large deflections. In addition, all except the first model incorporate the non-linear fillet material property. A curve of stress versus strain for this material is given in figure 3.5. The initial modulus of the fillet material is taken to be 1500 MPa.

3.3 CORRELATION OF FINITE ELEMENT LOAD-DEFLECTION CURVES WITH THE EXPERIMENTAL CURVE.

Graphs showing the load versus deflection (P/d) for each of the six models compared with the experimentally derived curve are shown in figures 3.6(a) to 3.6(f).

From figure 3.6(a) it can be seen that the initial full 2D undamaged model (Model 1) gives very similar values of deflection and hence initial stiffness to those obtained from the linear section of the experimental load-deflection curve. This is prior to any observed failure in the joint.

Model 2 results yield a stiffness of 1796 N/mm for a load of 5500 N, which is 20 % more than the equivalent value yielded from the experimental curve at this load. The P/d curve is still almost linear for the loads considered. This can be seen in figure 3.6(b).

The P/d curve generated for model 3 and given in figure 3.6(c) is beginning to show a certain amount of non-linearity.

When comparing models 3 and 4, it can be seen that there is very little stiffness reduction due to the increased amount of delamination in the overlaminate in model 4. This can be noted when comparing figures 3.6(c) and 3.6(d). The stiffness at a load of 10000 N for model 3 is 1762 N/mm and for model 4 is 1639 N/mm which is only a 7 % reduction. It can be noted that the deflections are very low when compared with the experimental values.

Model 5 represents the full damage scenario. It can be noted that for only a small amount of delamination between the web/overlaminate interface and the flange/overlaminate interface, there is a large reduction in stiffness to 1265 N/mm for a load of 19000 N. This is clearly seen when comparing figures 3.6(d) and 3.6(e). This value of stiffness is an 18 % reduction from the equivalent value for model 4 of 1548 N/mm. The deflections yielded from the modelling are approaching the equivalent experimental values.

In an attempt to achieve similar deflections as those obtained from experiment, model 6 was analysed which contains the same damage as model 5 but with further delaminations along the web/overlaminate and flange/overlaminate interfaces. This amount of delamination does give values of deflections close to the experimental values though there is still some difference, as can be seen from figure 3.6(f).

Three notable features from this consideration are:

(i) The stiffness of the finite element model is higher than that observed experimentally.

(ii) It is possible that internal damage occurred during the experiments which was not detectable by the naked eye. This would account for the sudden loss of stiffness at 8600 N which would, as a result, give rise to larger deflections for a given load.

(iii) It has been shown that an increase in the amount of interfacial delamination greatly increases the deflections. It is, therefore, possible that a certain amount of delamination between the web/overlaminate and flange/overlaminate may have occurred earlier than was visible with the naked eye.

(iv) Importantly, however, the trends of the numerically generated load-deflection curve mirror those generated experimentally and thus permit a qualitative assessment of the internal stress patterns.

3.4 STRESS RESULTS.

MODEL 1

The first sign of damage in the experiments was noted at 5500 N when the fillet was seen to crack. It was this value of load which was used to evaluate the theoretical deflection obtained from the undamaged model. This assesses the accuracy of the model. The results are given in table 3.4.

The results for fillet principal stress, overlaminate in-plane and through-thickness stresses are shown graphically in figures 3.7(a), 3.7(b) and 3.7(c) respectively.

The maximum value of fillet stress is 8.6 MPa which is not enough to cause failure since the ultimate tensile stress of the fillet material can be taken as 26.0 MPa (from ref. [5]). The maximum value occurs in the upper fillet corner where the overlaminate material meets the web and is shown in figure 3.7(a). If overlaminate through-thickness stresses are also taken into account, see figure 3.7(c), it can be noted that a delamination is likely along the web/overlaminate interface. In addition, the maximum value for the overlaminate through-thickness stress of 6.3 MPa which is enough to cause failure occurs near the lower fillet corner indicating likely delamination also along the flange/overlaminate interface.

The maximum value of in-plane stress in the overlaminate occurs on its outer surface near the centre. A value of 53 MPa is not enough to cause failure since the in-plane strength of the overlaminate material is taken to be 207 MPa.

It is also noted that the top of the web moves horizontally by 0.16 mm. This is consistent with the experimental observations in which the joint web was seen to bend away from the damage side.

MODEL 2

Only the fillet crack was seen in the experiments but it is likely that a small debond would have occurred first as this would induce higher stresses in the fillet causing it to fail. Results have been obtained for this model at five different load levels and are given in table 3.5.

Typical plots of fillet principal stress, overlaminate in-plane and through-thickness stresses are shown in figures 3.8(a), 3.8(b) and 3.8(c) respectively.

For a load of 5500 N figure 3.8(a) shows that the maximum value of S1 in the fillet again occurred in the upper fillet corner indicating delamination along the interface in this region is likely. S1 max. is lower than the fillet U.T.S. of 26.0 MPa. The strains in the fillet are also very low. The stress and strain levels at each load given in table 3.5, are consistent with the values taken from the stress/strain curve given in figure 3.5.

It is also worth noting that the elastic modulus of the fillet is still its linear region.

The maximum values of SX and SY in the overlaminate are in similar regions as model 1.

As the load is increased, the stress patterns and hence the stress distributions for S1 in the fillet and SX and SY in the overlaminate are consistent with those already discussed.

MODEL 3

This model represents the debond, crack in fillet and first delamination. The results are given in table 3.6.

It can be noted that the values of horizontal deflection are gradually decreasing for the higher loads. This indicates that at these loads the tip of the web is actually bending back towards the damage side by a small amount.

Typical plots of fillet principal stress, overlaminate in-plane and through-thickness stresses are given in figures 3.9(a), 3.9(b) and 3.9(c) respectively.

For a load of 5500 N the maximum principal stress in the fillet occurs in the upper fillet corner on the damage side of the model as before. High values of S1 are obtained in the upper fillet corner on the non-damage side. The region of maximum stress appears to be smaller than in the case of model 2 which is shown in figure 3.8(a).

It can be noted that for strain levels up to 0.013 strain, the equivalent stress levels are consistent with a modulus of approximately 1500 MPa. This shows that the fillet material is behaving in linear fashion up to these strain levels. At higher strains its behaviour, however, is clearly non-linear.

The maximum value of SX in the overlaminate is in a similar region as model 2.

The maximum value of SY in the overlaminate occurs at the upper end of the inserted delamination. The magnitude of this stress was 52 MPa which seemed high in comparison with the equivalent value at the lower end of the delamination of about 25 MPa. The reason for this high value is that no explicit failure criterion was set in the models used here. Hence a value higher than the interlaminar tensile strength indicates failure in a qualitative sense.

As the load is increased the stress patterns and hence the stress distributions for S1 in the fillet and SX and SY in the overlaminate are consistent with those already discussed.

MODEL 4

This model represents the debond, crack in fillet and further delaminations. The results are shown in table 3.7.

The negative value for horizontal deflection indicates that the web tip is moving by a small amount in a direction towards the damage side. This is a similar result to the results of model 3.

Typical plots of fillet principal stress, overlaminate in-plane and through-thickness stresses are given in figures 3.10(a), 3.10(b) and 3.10(c) respectively.

For a load of 10000 N the maximum fillet principal stresses occur in the region of the lower fillet corner, again indicating that delamination along the flange/overlaminate interface is possible. This is shown in figure 3.10(a). The magnitude of the maximum S1 is approaching the failure load of the fillet.

The maximum value of SX in the overlaminate is in a similar region as model 3. The actual stress distribution is given in figure 3.10(b). Failure due to overlaminate in-plane stresses would not occur at this load.

The maximum value of overlaminate through-thickness stress occurs near the ends of the inserted delaminations and their magnitude is enough to indicate propagation.

For a load of 15000 N the principal stress distribution in the fillet is the same as at a load of 10000 N except that there is an additional high stress region in the upper fillet corner on the non-damage side. This is shown in figure 3.10(d).

The principal stress distribution in the fillet at a load of 19000 N is the same as at a load of 15000 N except that there is an additional high stress region in the lower fillet corner on the non-damage side.

The maximum values of SX and SY in the overlaminate are in similar regions as before.

MODEL 5

This model represents the completely damaged joint as observed from experiments at the failure load of 19000 N. The results are given in table 3.8.

Typical plots of fillet principal stress, overlaminate in-plane and through-thickness stresses are given in figures 3.11(a), 3.11(b) and 3.11(c) respectively.

Figure 3.11(a) shows that at a load of 5500 N the maximum principal stress in the fillet occurs in the lower region of the fillet. A region of high principal stress also occurs at the lower end of the inserted crack. The discontinuous nature of the stress contours in this region shows that this is likely to be

due to a singularity.

The highest value of the through-thickness stress in the over-laminate occurs at the upper end of the interfacial delamination between the web and the over-laminate as shown in figure 3.11(c). There are also regions of high stress at the end of the delamination between the flange and the over-laminate. Regions of medium stress occur in the central regions of the over-laminate where the delaminations are present. The stresses in these regions are of such magnitude to suggest that the delaminations would propagate.

The stress distributions resulting from higher loads are consistent with those already discussed. It should also be noted that there are also regions of high fillet principal stresses in the upper and lower fillet corners on the non-damage side at a load of 17000 N. This is shown graphically in figure 3.11(d).

MODEL 6

Typical plots of fillet principal stress, overlaminate in-plane and through-thickness stresses are shown in figures 3.12(a), 3.12(b) and 3.12(c) respectively.

The stress distributions yielded from this analysis are similar to those generated for model 5. There are a number of interesting points to note, however. At a load of 5500 N and thereafter, there is a region of high through-thickness stress in the over-laminate at the interface where the edge of the over-laminate joins the flange. This indicates likely delamination in this region. This is shown in figure 3.12(c). In addition at 13000 N, the maximum fillet stress occurs in the lower fillet corner on the damage side. This is shown in figure 3.12(a) and indicates that delamination along the overlaminate/flange interface is possible.

3.5 COMPARISON OF FINITE ELEMENT STRESS PATTERNS WITH EXPERIMENTAL FINDINGS.

MODEL 1

At a load of 5500 N the high stresses in the upper fillet corners indicate that damage is likely along the web/over-laminate interface. Figure 3.7(a) shows this region of high stress. The resulting stresses in the fillet at a load of 5500 N of 9 MPa are not enough to fail the fillet material which has a UTS of 26.0 MPa. It is possible that either an initial flaw or void was already present in the fillet due to fabrication processes. This flaw may have caused premature failure in the joints.

The highest values of through-thickness stress in the over-laminate occurs in the lower three to four layers of the over-laminate in two distinct regions as shown in figure 3.7(c). This is consistent with the delaminations which were later seen in the experiments.

MODEL 2

Load = 5500 N

The through-thickness stress distribution is similar to that for model 1 at this load (figure 3.8(c)) and indicates that the delamination would progress.

Load = 7500 N

This is the load at which the first signs of delamination were visible. High through-thickness overlaminate stresses occur near the lower fillet corner, indicating that there could be delamination along the flange/overlaminate interface.

MODEL 3

Load = 7500 N

High regions of through-thickness overlaminate stresses occur in the central regions of the overlaminate where the delaminations are present indicating that further damage in these regions is likely.

Load = 10000 N

A much greater region of high through-thickness overlaminate stresses is present which is consistent with the observed failure at this load indicating numerous delaminations in this region.

MODEL 4

Load = 10000 N and 19000 N

Regions of high through-thickness over-laminate stresses indicate that interfacial delaminations are likely along the web/over-laminate and flange/overlaminate interfaces which was later seen in the experiments.

MODEL 5

Load = 19000 N

As above, regions of high through-thickness overlaminate stresses indicate that interfacial delaminations are likely along the web/overlaminate and flange/overlaminate interfaces which was later seen in the experiments.

3.6 DISCUSSION.

The load-deflection curve was modelled satisfactorily. The numerical results did not give as much deflection for a given load as in the experiments. This could be due to a number of reasons. It is possible that damage was present in the joint prior to loading, due to such factors as fabrication technique and method of fillet injection. Voids may have been present in the fillet which would account for its premature failure at apparently low stresses.

The values of horizontal deflections are consistent with the observed experimental behaviour in which the joint was seen to bend away from the damage side. At higher loads for model 3, the web tip bends away from the damage side by a smaller amount than at lower loads. In addition, at the highest load for model 4 the web bends towards the damage side. It should be noted that no damage in these two models was inserted between the overlaminate and the web. It is possible that since there is only damage on one side of the joint, at higher loads the increased stiffness on the non-damage side prevents the joint from moving as far in the horizontal direction than at lower loads. The vertical deflection of the web, however, increases as the load increases as would be expected. Model 5, however, contains delaminations along the overlaminate/web interface and the overlaminate/flange interface. Due to the increase in damage, the web is less restricted in its movement horizontally.

It is likely that there was internal damage which was not visible during the experiments. In addition, it is possible that there was more delamination along the web/overlaminate and flange/overlaminate interfaces than was visible during the tests. This would account for the increased flexibility and hence deflection of the joint for a given load.

The assumed material properties may not correctly represent the actual values of the materials used in the joint. If the stiffnesses of the materials were over-estimated then this would explain the lower values of deflection obtained for given load levels.

Due to modelling constraints, the applied model boundary conditions may not correctly represent the actual experimental set-up. A boundary condition sensitivity study shall be carried out in the near future.

Stresses in the fillet seem to be low and not adequate to cause the experimentally observed failure. As indicated earlier, the fillet failure may have been due to imperfections or flaws. Importantly, stress patterns in the overlaminate seem to adequately mirror the damage scenario seen in the experiments.

4. THE USE OF FRACTURE MECHANICS - A PRELIMINARY STUDY.

4.1. J-INTEGRAL EVALUATION.

The J-integral is defined as a path-independent line integral that measures the strength of the singular stresses and strains near a crack tip.

$$J = \int_{\Gamma} W dy - \int_{\Gamma} \left(t_x \frac{\delta u_x}{\delta x} + t_y \frac{\delta u_y}{\delta y} \right) ds \qquad (3)$$

where: Γ = any path surrounding the crack tip

W = strain energy density (strain energy per unit volume)

t_x = traction vector along x-axis $(\sigma_x n_x + \sigma_{xy} n_y)$

t_y = traction vector along y-axis $(\sigma_y n_y + \sigma_{xy} n_x)$

σ = component stress

n = unit outer normal vector to path Γ

u = displacement vector

s = distance along path Γ

For linear elastic problems the J-integral can be assumed to be equivalent to the strain energy release rate G. The crack is said to propagate if the value of G is greater than a critical value of strain energy release rate G_c.

4.2 FINITE ELEMENT MODEL.

The 2D T-Joint model used previously has been modified in order to incorporate fracture mechanics criteria so as to study crack propagation. The T-Joint is assumed to be composed of one isotropic material whose material properties are as follows:

$E = 10000$ MPa
$\upsilon = 0.25$

The T-Joint is loaded in three-point bending as before.

Due to the symmetry of the loading and the geometry, only half the joint has been modelled. In addition, plane strain conditions are assumed to exist since the joints can be assumed to be wide in relation to their thickness and length.

In linear elastic problems it is assumed that the displacements near the crack tip vary as $1/\sqrt{r}$ where r is the distance from the crack tip. As a result, the stresses and strains are singular at the crack tip (where $r = 0$). 2D singular elements are used around the crack tip which are able to pick up the singularity in the strain. The whole T-Joint was meshed automatically with 2D plane strain elements. For each model, a crack was inserted in the T-joint at the corner of the fillet between the overlaminate and the flange. The model can be seen in figure 4.1. It was also necessary to insert gap elements between the nodes along the crack. This was necessary to ensure that the two crack surfaces did not cross over each other which would obviously not occur in reality. The compressive stiffnesses of the gap elements was set to be 10^6 MPa for this reason. Their stiffnesses in tension was zero so as not to inhibit the crack should it open. A displacement check on selected nodes to confirm that the two crack surfaces did not cross over each other was carried out, the results of which are discussed in section 3.3

A total of three different models were analysed:

(A)	10 mm crack	
(B)	10 mm crack	J-integral calculated along a different path to confirm its path independency
(C)	10 mm crack	Values of E and υ changed to be 14680 MPa and 0.123 respectively to quantify material property dependency

A typical plot of the crack tip element and the path used to calculate the J-integral value is shown in figure 4.2.

4.3. RESULTS.

An initial check on the nodal displacements along the crack was necessary to ensure that the crack tended to open out and that the two faces did not cross over each other. This was carried out by noting the displacements for two sets of coincident nodes and ensuring that the vertical displacement (y direction) for the top nodes was higher than that for the equivalent bottom nodes. This was done for model A and the results are shown in table 4.1.

From table 4.1 it can be noted that the top nodes have a greater displacement than the equivalent bottom nodes. This shows that the inserted gap elements ensure that the crack opens out correctly.

The J-integral results of all three models A to C are given in table 4.2

Comparing models A and B it can be seen that the values of the J-integral are very similar. This supports the path independent nature of the J-integral.

Comparing models A and C, it is shown that by increasing the modulus and reducing the Poisson ratio of the material, the value of the J-integral reduces. This indicates that for a given loading condition a crack of a given length is less likely to propagate in a structure which has an increased modulus and Poisson ratio.

5. FURTHER WORK.

Three avenues are of potential interest and worth investigating.

(i) The first concerns delaminations in plate structures. The work upto now has focussed on long-thin beams of very large aspect ratios. There is a need to extend this to more realistic plates of smaller aspect ratios. Further work will therefore attempt to parametrically study variations in: (a) delamination zone area vis-a-vis overall plate area; (b) delamination zone width vis-a-vis plate width; (c) plate boundary conditions.

(ii) The second concerns stress modelling in T-joints. Current work has looked at one configuration under a three-point bending model. However, it is known that other load configurations could present more extreme responses, e.g. 45° pull-off. So a comparison can be made between published evidence on the 45° pull-off results and the present three-point bend test results. Also, it is worth noting that in a practical context ship staff and onshore survey staff are only likely to note the location and length of delamination in a joint. So it may be worth studying the load carrying capacity of T-joints (in the form of stress patterns for a given limiting load) for a series of delaminations varying in length and through the thickness of the overlaminate.

(iii) Finally the fracture study of the isotropic T-joint will be extended to cover a full 2D model which incorporates all the constituents and their material properties. It is proposed to evaluate the J-integral for a variety of (delamination) crack scenarios, as mentioned in (ii) above, and compare it with the critical strain energy release rates.

6. CONCLUDING REMARKS.

(i) A refined FE model has been used to predict critical buckling stresses for delaminated beam specimens. The results are consistent with experimental values. This modelling approach therefore presents a potential way ahead for examining structure panels, of finite aspect ratios, with embedded delaminations.

(ii) A reasonably good correlation has been achieved between the numerical modelling of T-joints and the experimental load-deflection results. The FE model, as is to be expected, is somewhat stiffer than the test specimen. Some of the potential causes for the variations have been explored. The FE model was also used to generate stress patterns at a variety of load steps. Stresses in the fillet corresponding to the experimentally observed fillet failure load are shown to be low. The observed failure in the tests could therefore have been due to imperfections in the specimen. Through-thickness stresses in the overlaminate on the other hand, have come out to be high at loads and locations where delaminations have been observed. Hence it is possible to estimate the progression of damage in at least a qualitative manner.

(iii) The preliminary investigation into the use of the J-integral approach has been successful in the case of the idealised, isotropic T-joints. This presents a possible avenue for further investigation vis-a-vis delamination cracks in FRP T-joints.

7. REFERENCES.

1. Phillips, H. J. & Shenoi, R. A.. Analytical Modelling Concerning onset of Delamination in FRP Beam Panels. University of Southampton, Department of Ship Science. Ship Science Report No. 82, March 1994.

2. Phillips, H. J. & Shenoi, R. A.. Modelling the Compressive Behaviour of Delaminated Beams using a Finite Element Technique. University of Southampton, Department of Ship Science. November 1994.

3. Sumpter, J. D. G. & Lay, P. W.. A Study of through width Delaminations in Compressively Loaded GRP. DRA/SMC/CR943120. Dec. 1994.

4. Elliot, D. M.. Mechanical Testing of Composite Joints - Interim Report. DRA/AW/AWS/TR94212. April 1994.

5. Shenoi, R. A. & Hawkins, G. L.. Influence of material and geometry variations on the behaviour of bonded tee connections in FRP ships. Composites. Volume 23. Number 5. September 1992. pp 335-345.

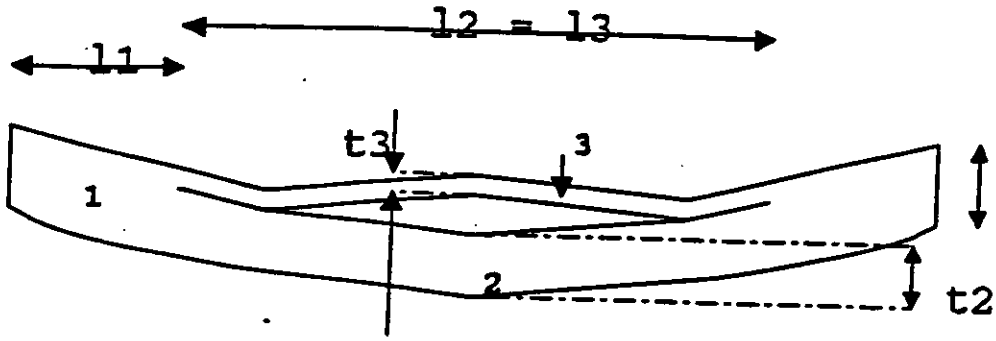

Figure 2.1 Model of three parts of a Delaminated Beam.

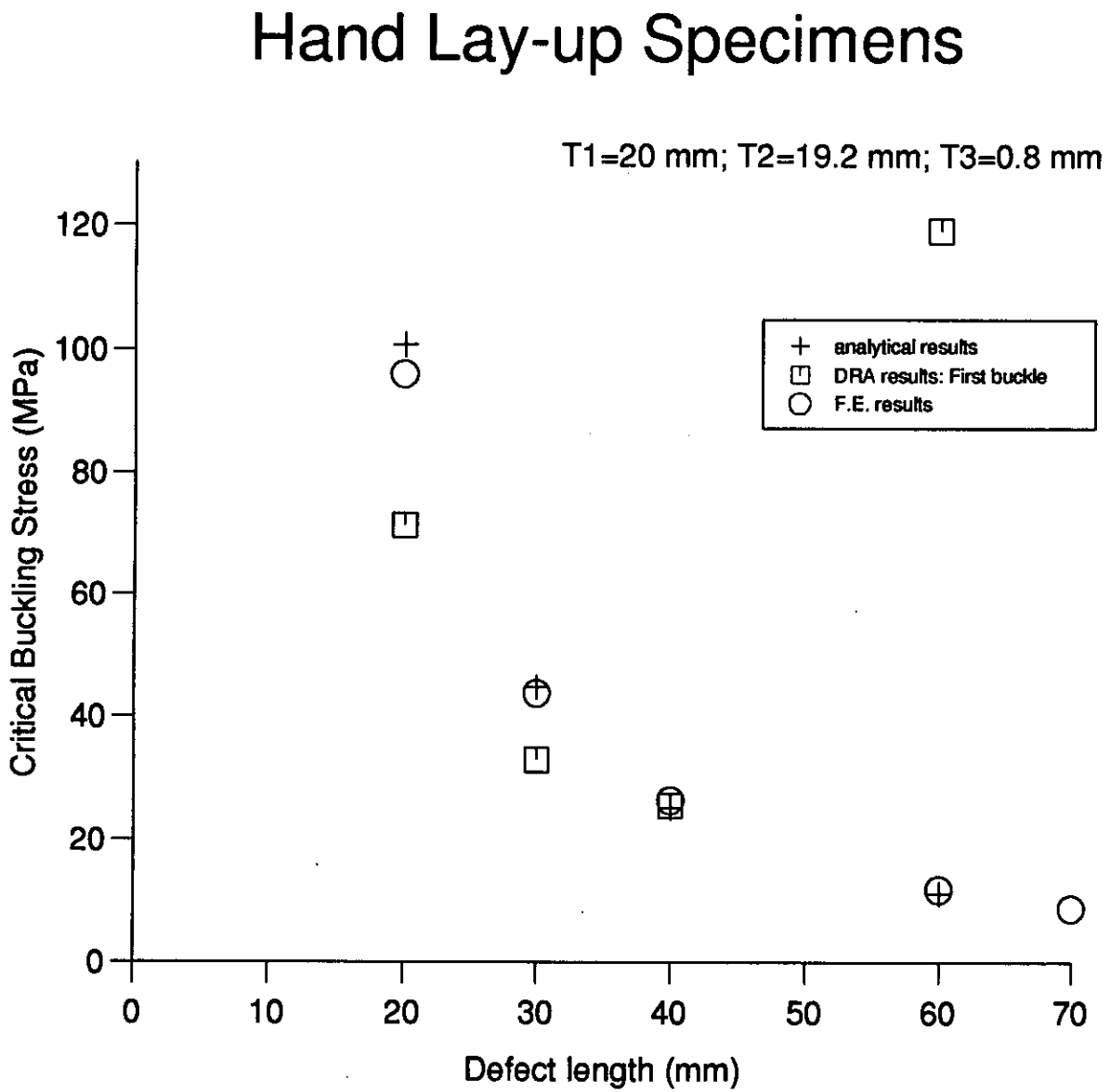

Figure 2.2(a) Hand Lay-up Specimens with defect 1 ply deep. Critical Buckling Stress vs. Defect Length.

Hand Lay-up Specimens

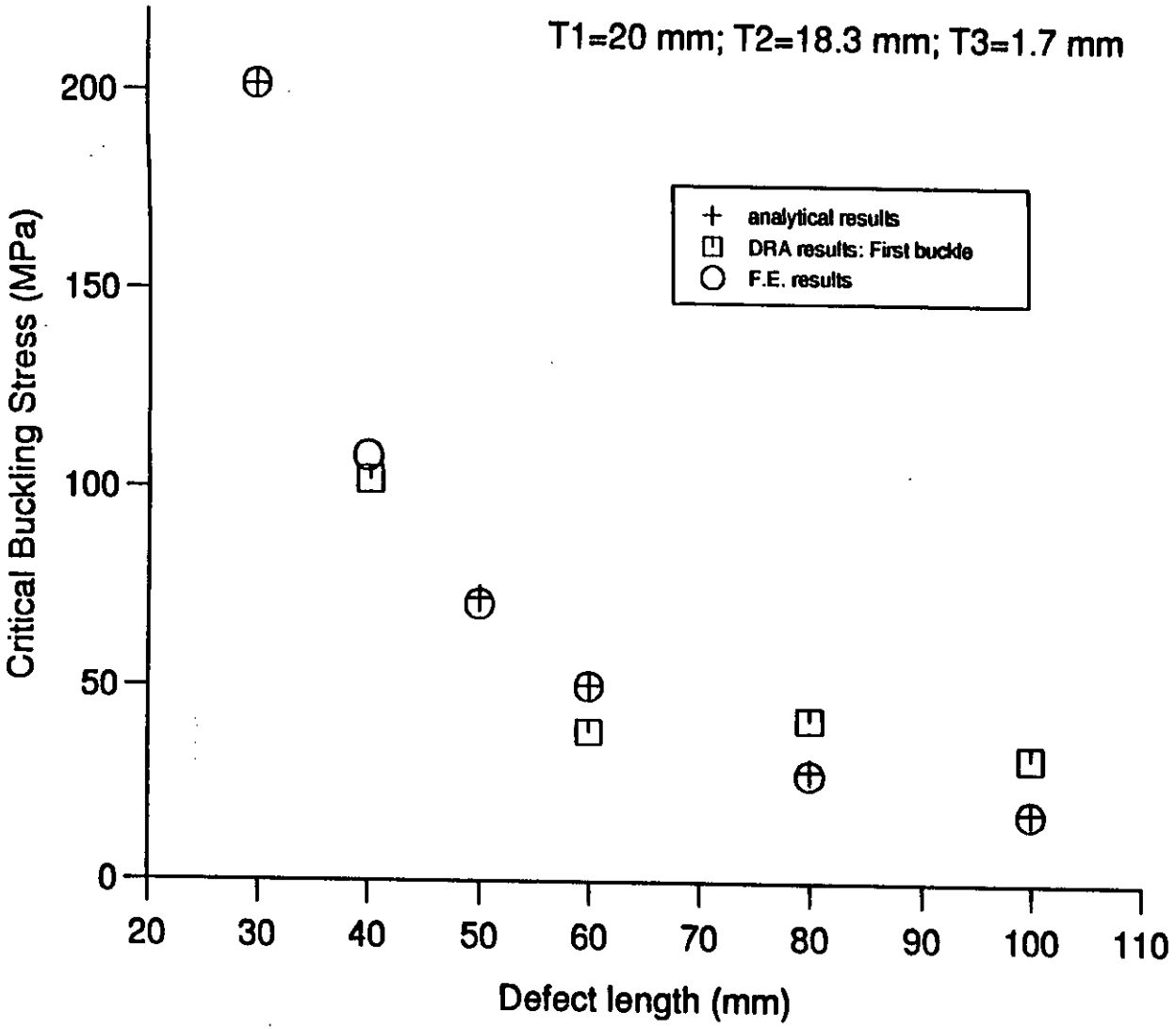

Figure 2.2(b) Hand Lay-up Specimens with defect 2 plies deep. Critical Buckling Stress vs. Defect Length.

Hand Lay-up Specimens

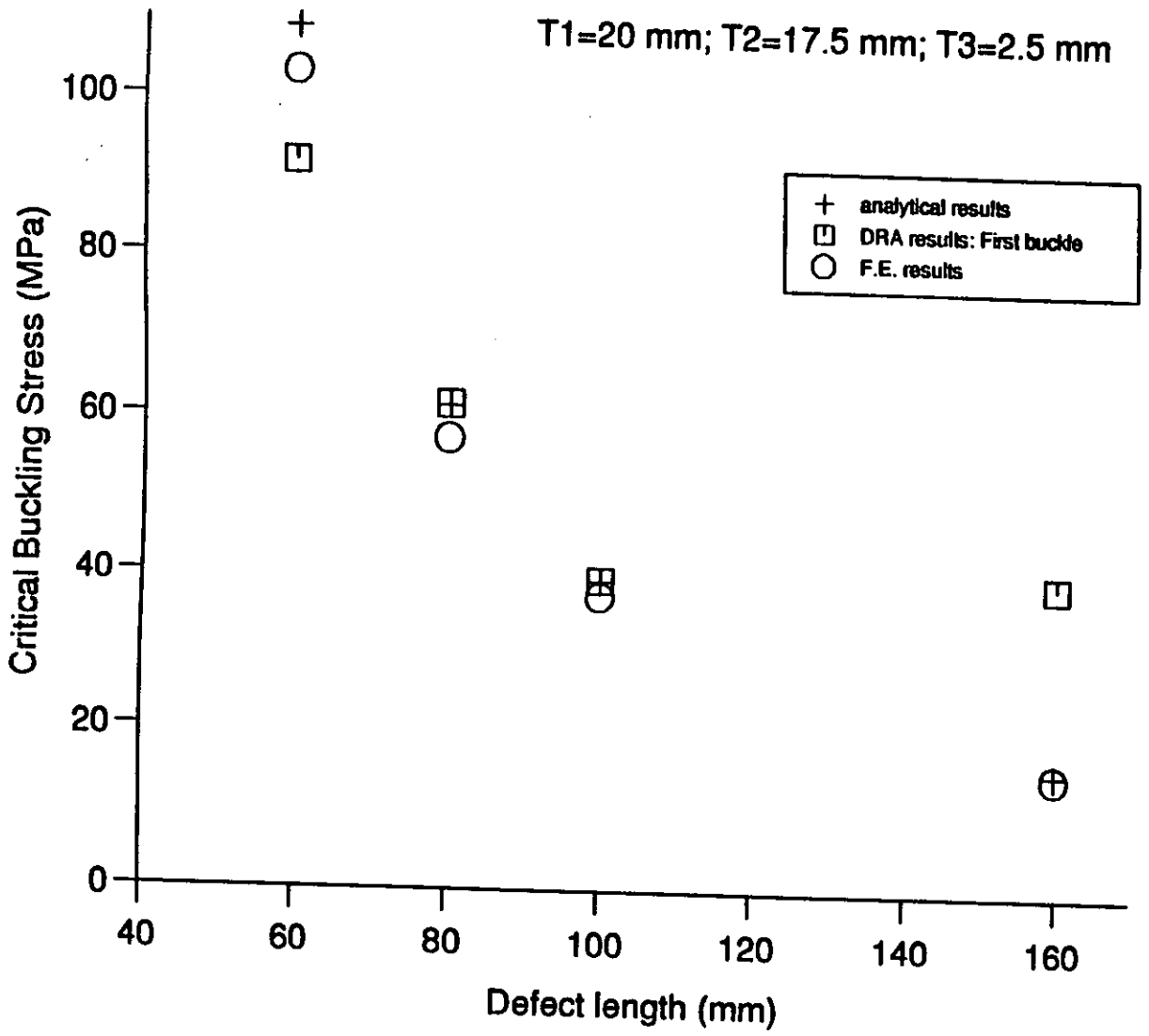

Figure 2.2(c) Hand Lay-up Specimens with defect 3 plies deep. Critical Buckling Stress vs. Defect Length.

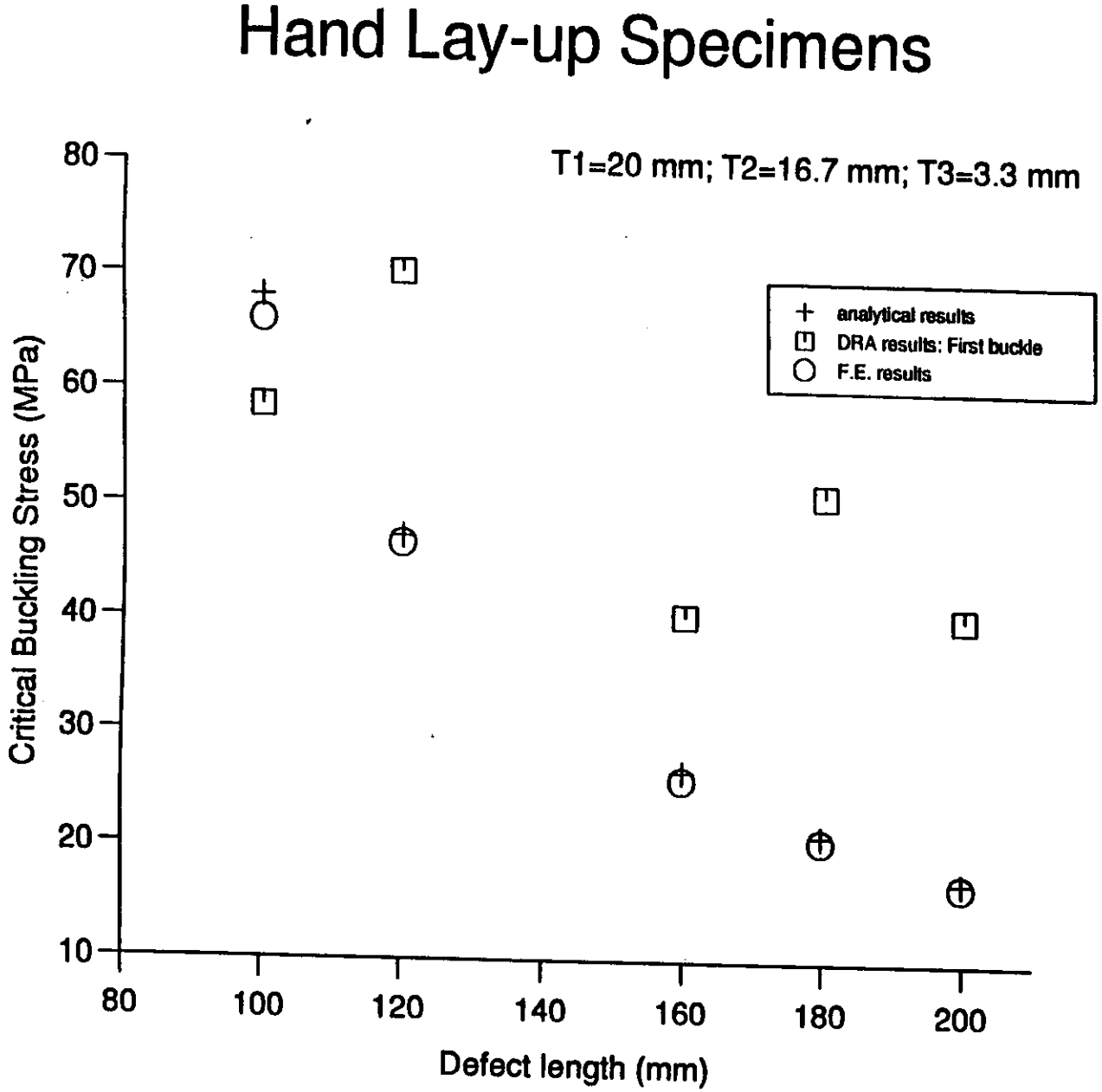

Figure 2.2(d) Hand Lay-up Specimens with defect 4 plies deep. Critical Buckling Stress vs. Defect Length.

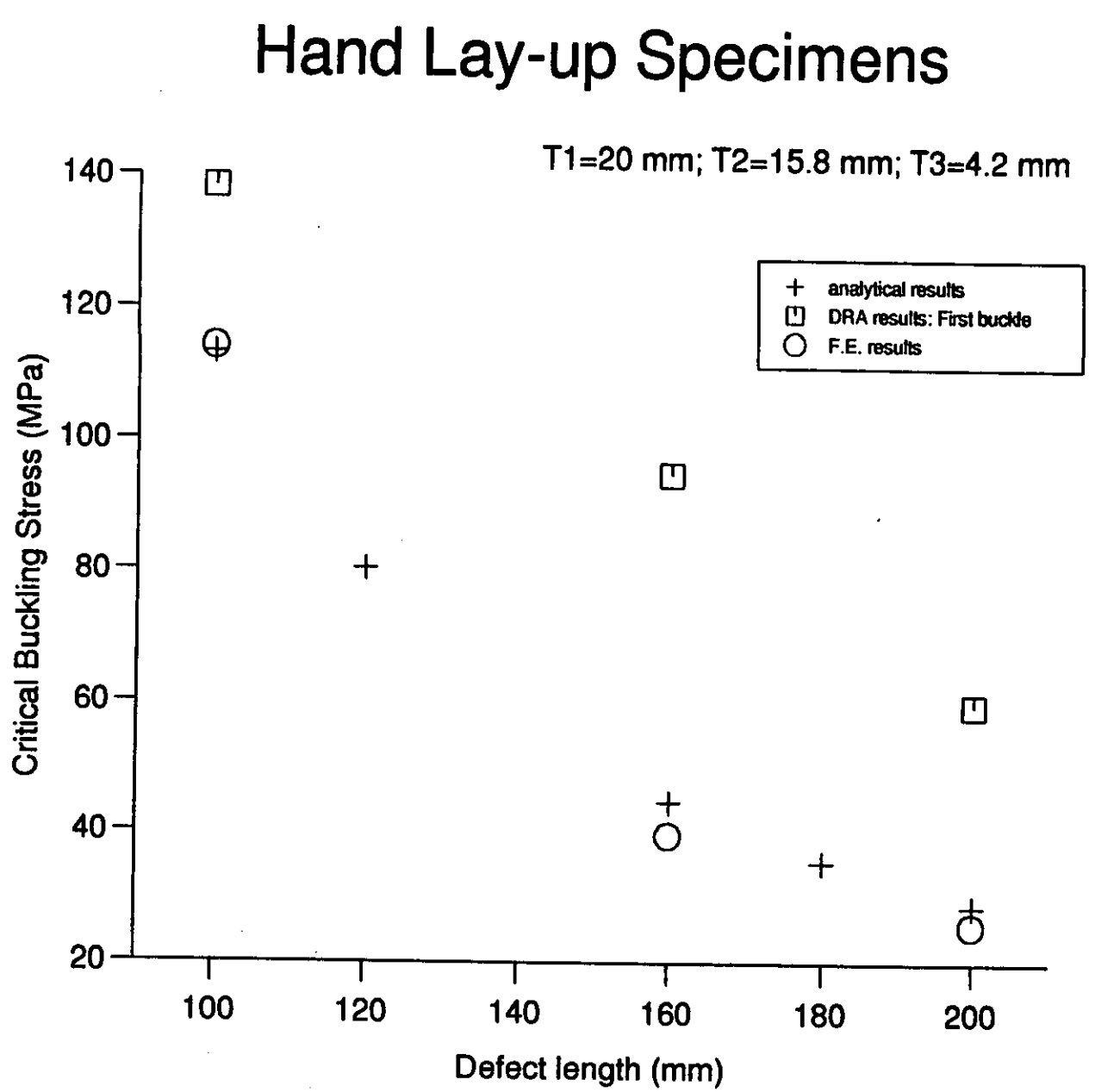

Figure 2.2(e) Hand Lay-up Specimens with defect 5 plies deep. Critical Buckling Stress vs. Defect Length.

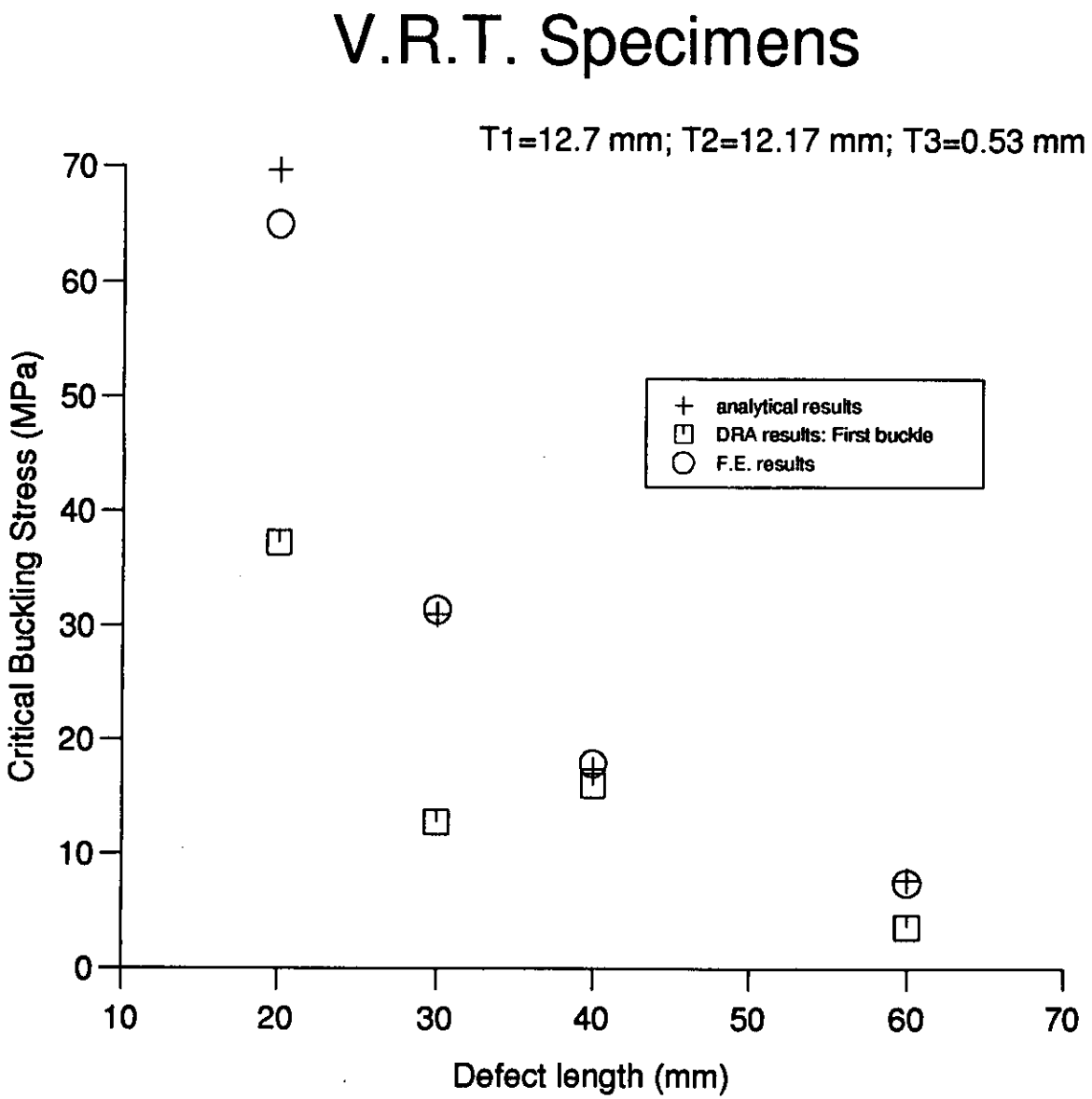

Figure 2.3(a) Hand Lay-up Specimens with defect 1 ply deep. Critical Buckling Stress vs. Defect Length.

V.R.T. Specimens

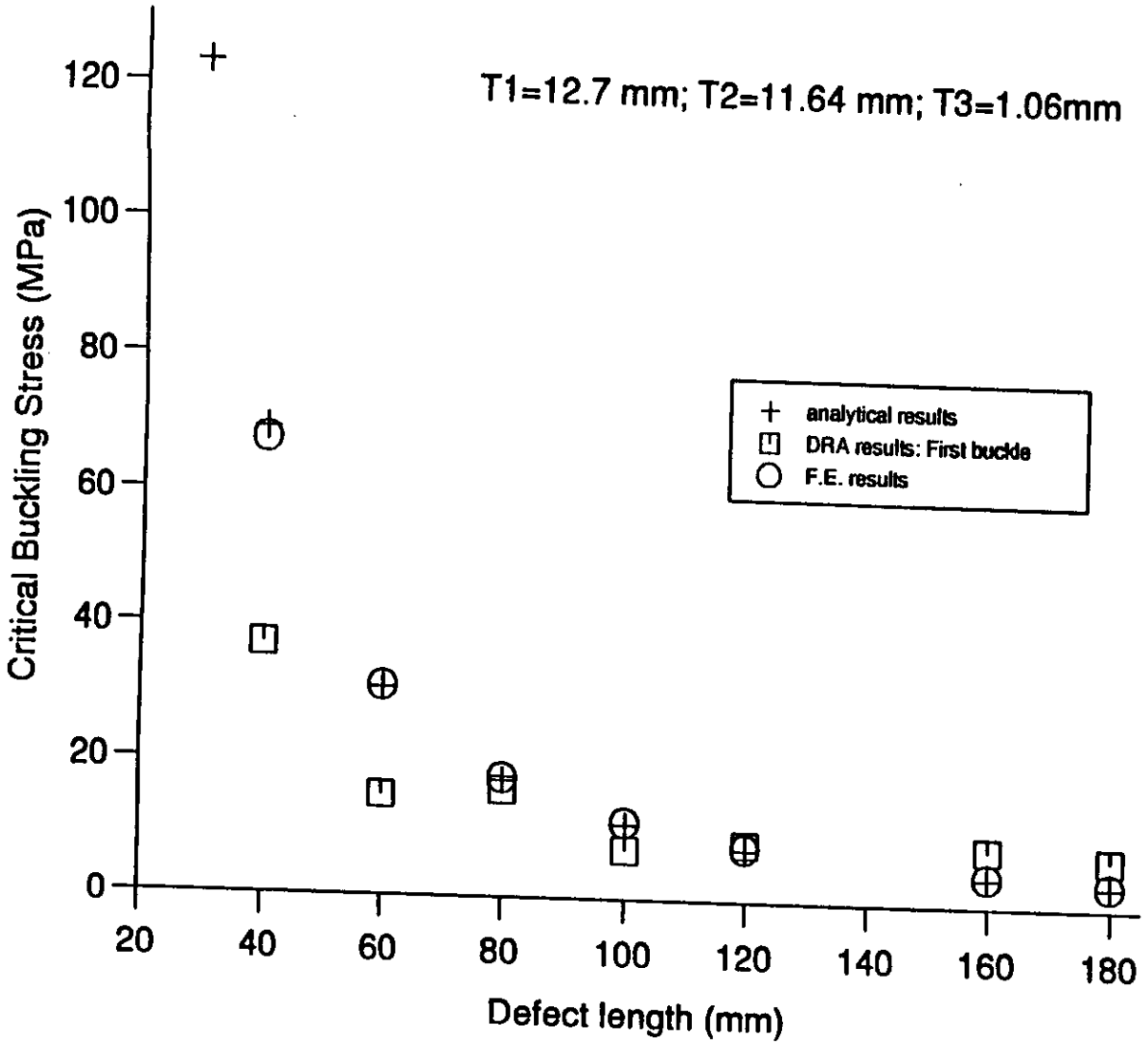

Figure 2.3(b) Hand Lay-up Specimens with defect 2 plies deep. Critical Buckling Stress vs. Defect Length.

V.R.T. Specimens

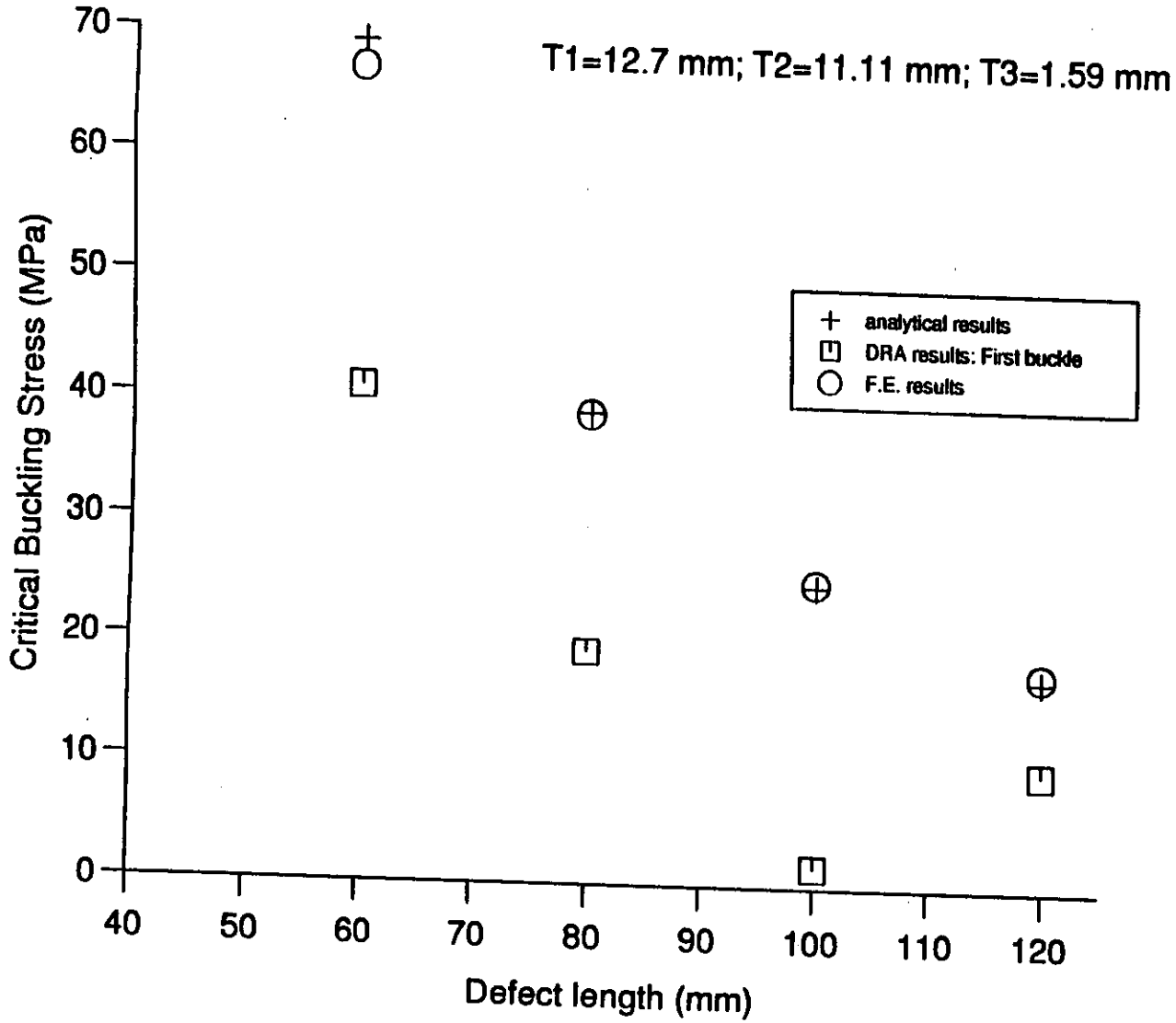

Figure 2.3(c) Hand Lay-up Specimens with defect 3 plies deep. Critical Buckling Stress vs. Defect Length.

V.R.T. Specimens

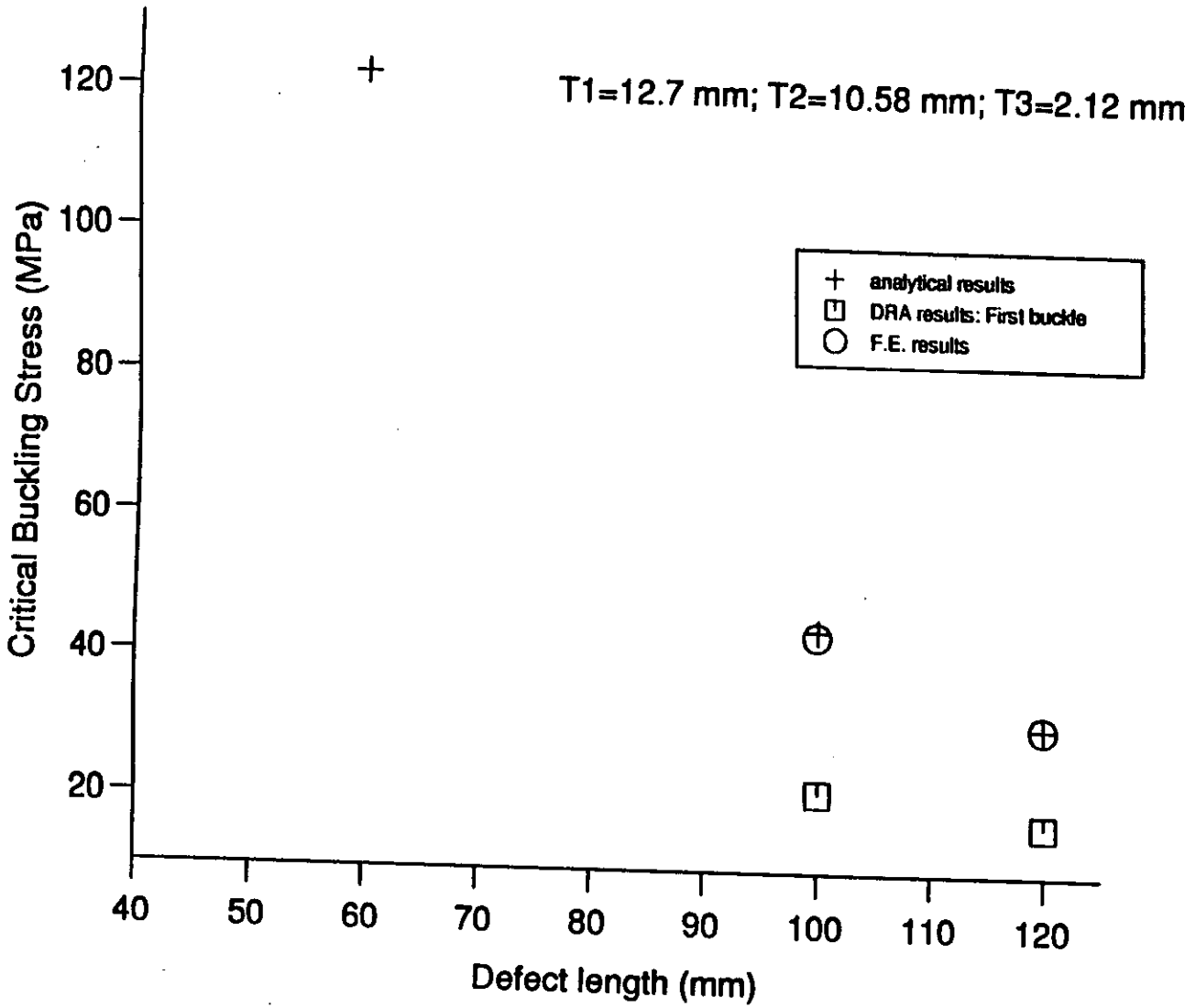

Figure 2.3(d) Hand Lay-up Specimens with defect 4 plies deep. Critical Buckling Stress vs. Defect Length.

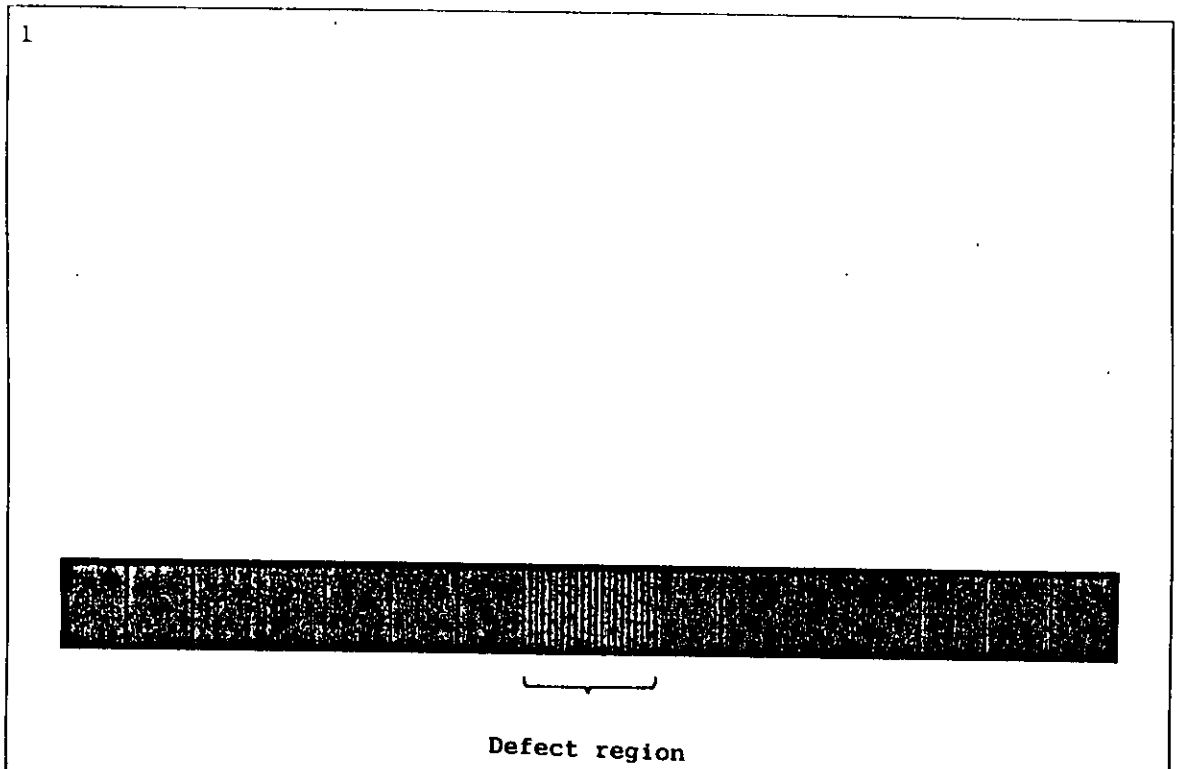

Figure 2.4 Defect Region in Finite Element Delaminated Beam Model.

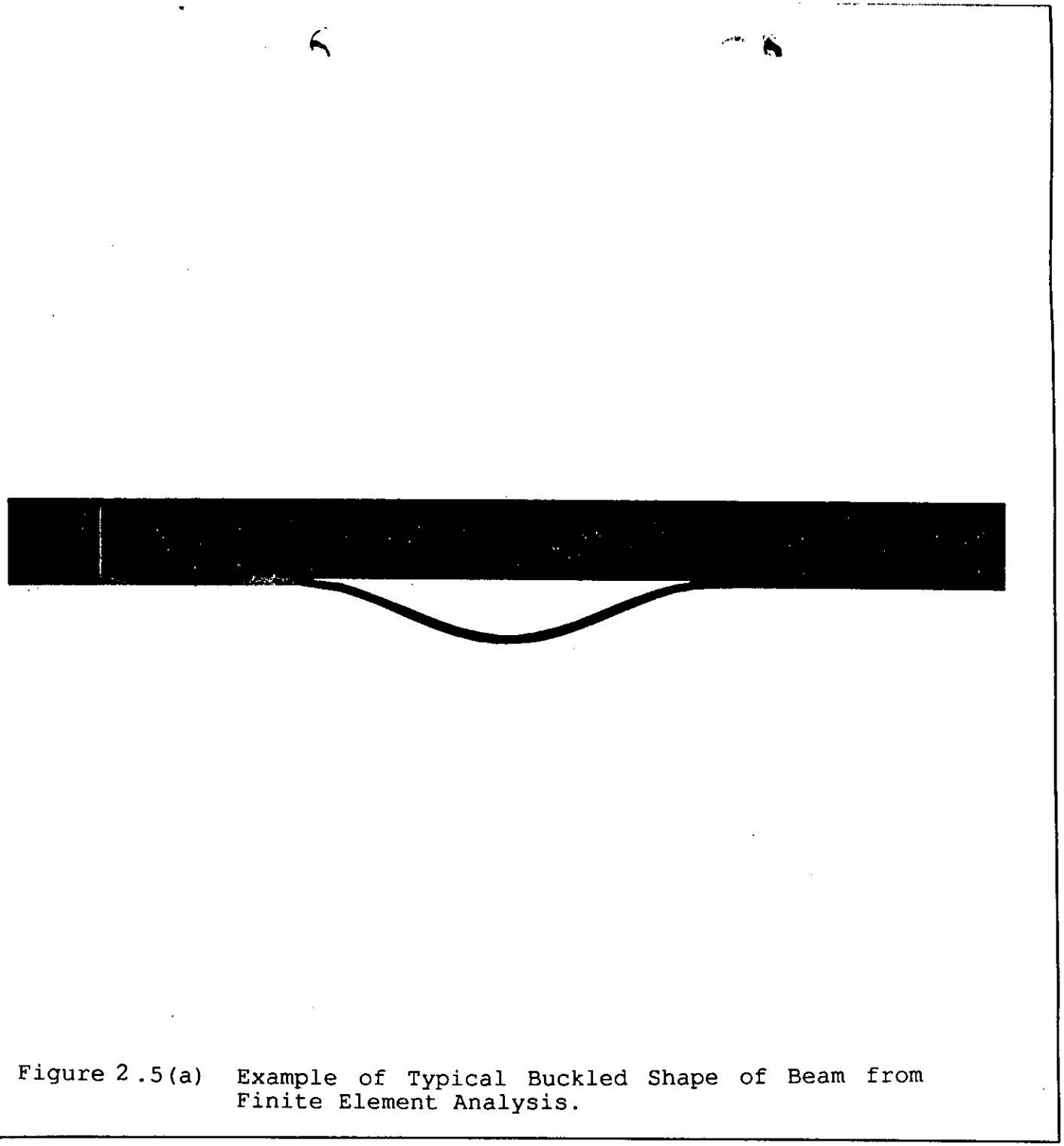

Figure 2.5(a) Example of Typical Buckled Shape of Beam from Finite Element Analysis.

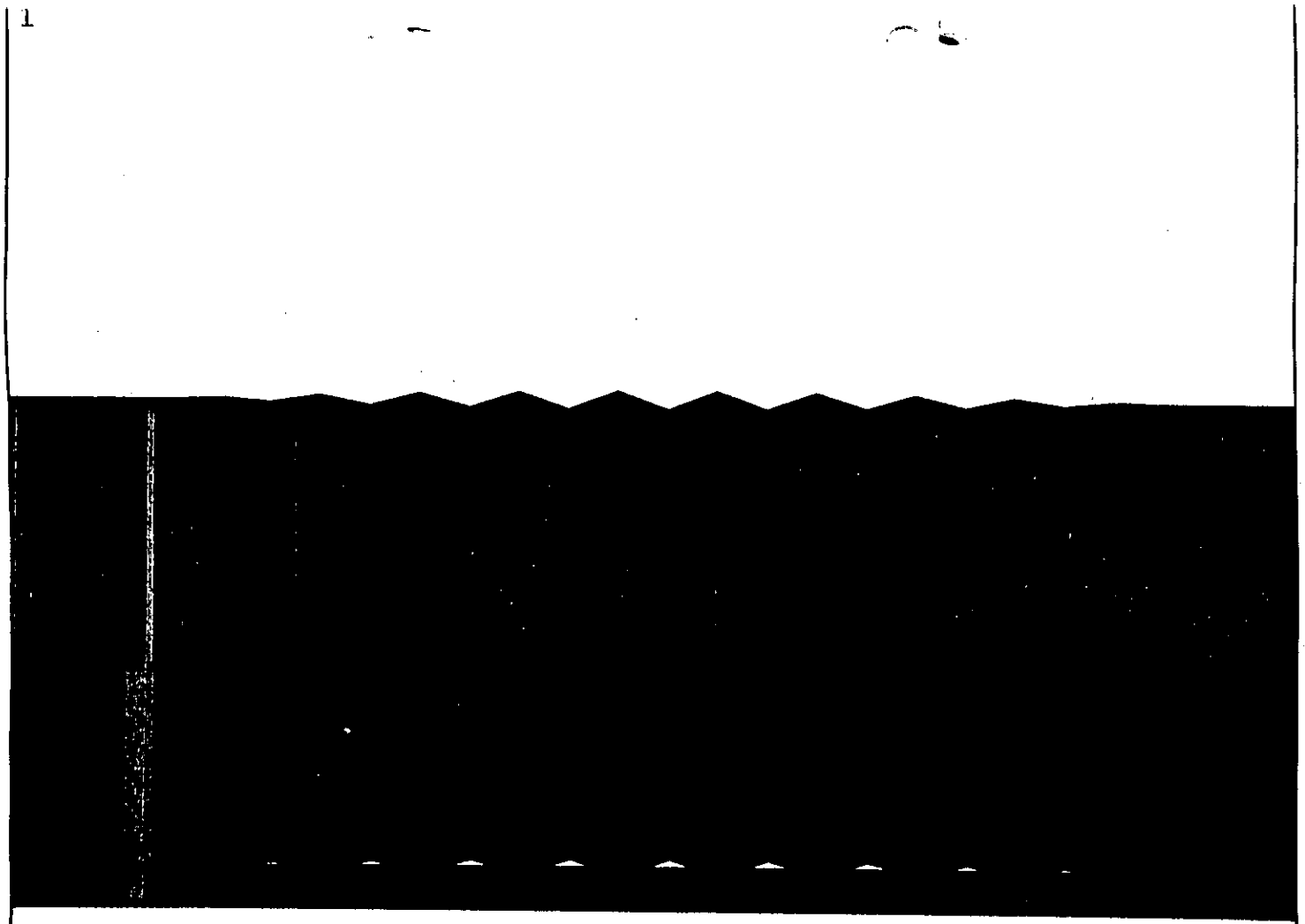

Figure 2.5(b) Example of Non-Typical Buckled Shape of Beam from Finite Element Analysis.

ANSYS 5.0 A 20
APR 27 1995
12:25:45
PLOT NO. 1
ELEMENTS
TYPE NUM

ZV =1
DIST=132
XF =120
YF =10
CENTROID HIDDEN

Figure 2.6 Finite Element Model generated using Automatic Meshing.

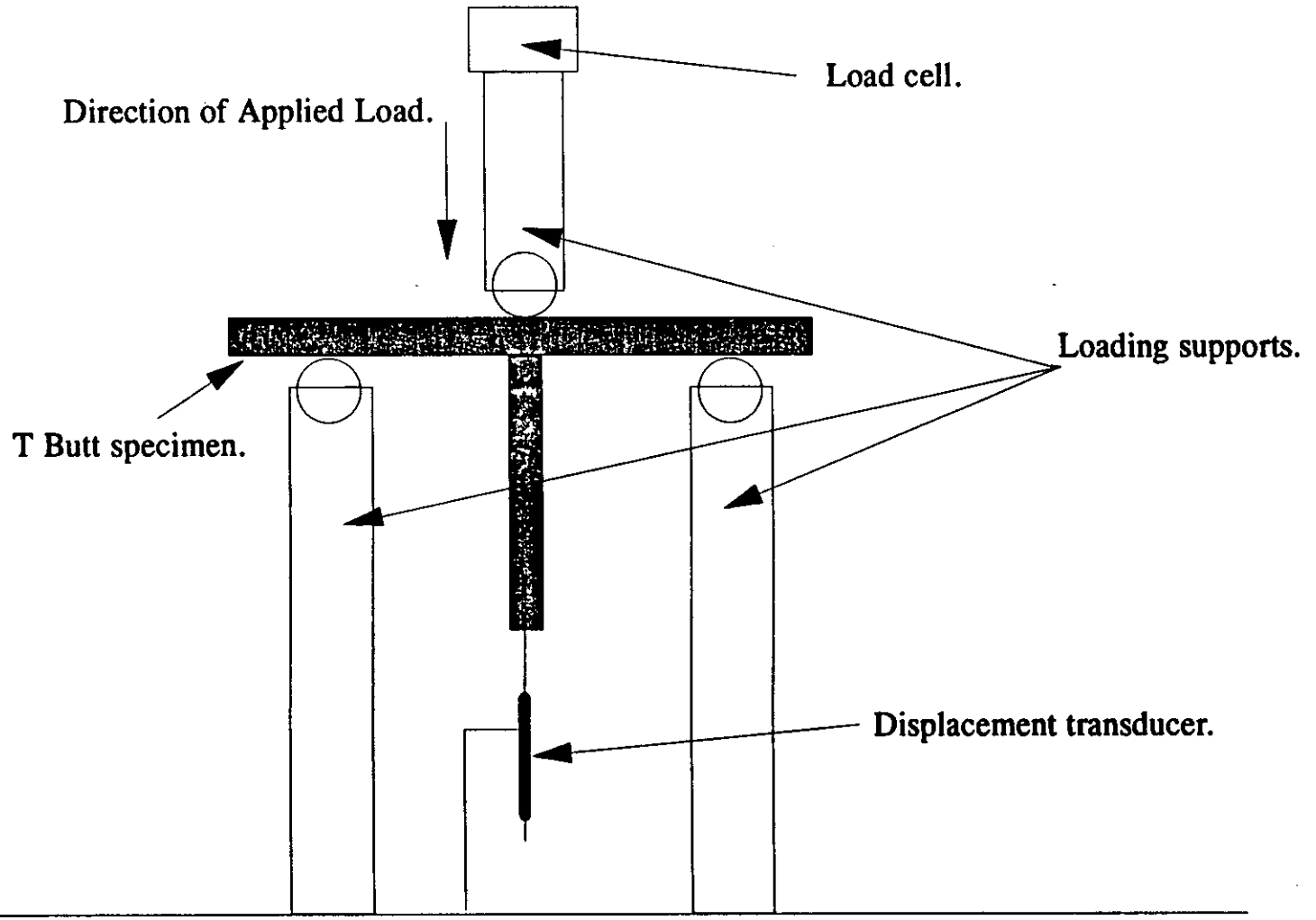

Figure 3.1 Loading Set-up used in T-Joint Three-Point Bending Tests.[4]

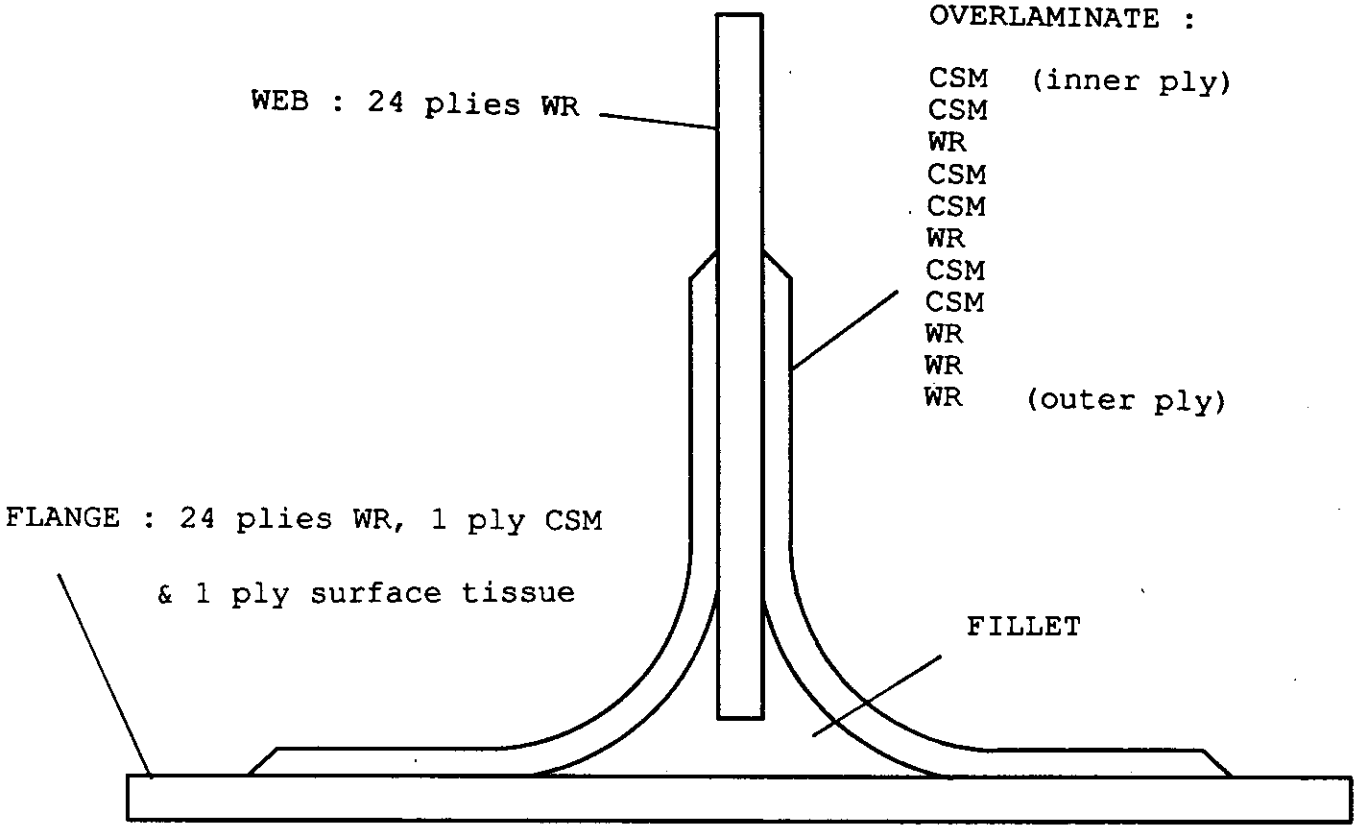

Figure 3.2 Schematic of materials used in T-Joints.

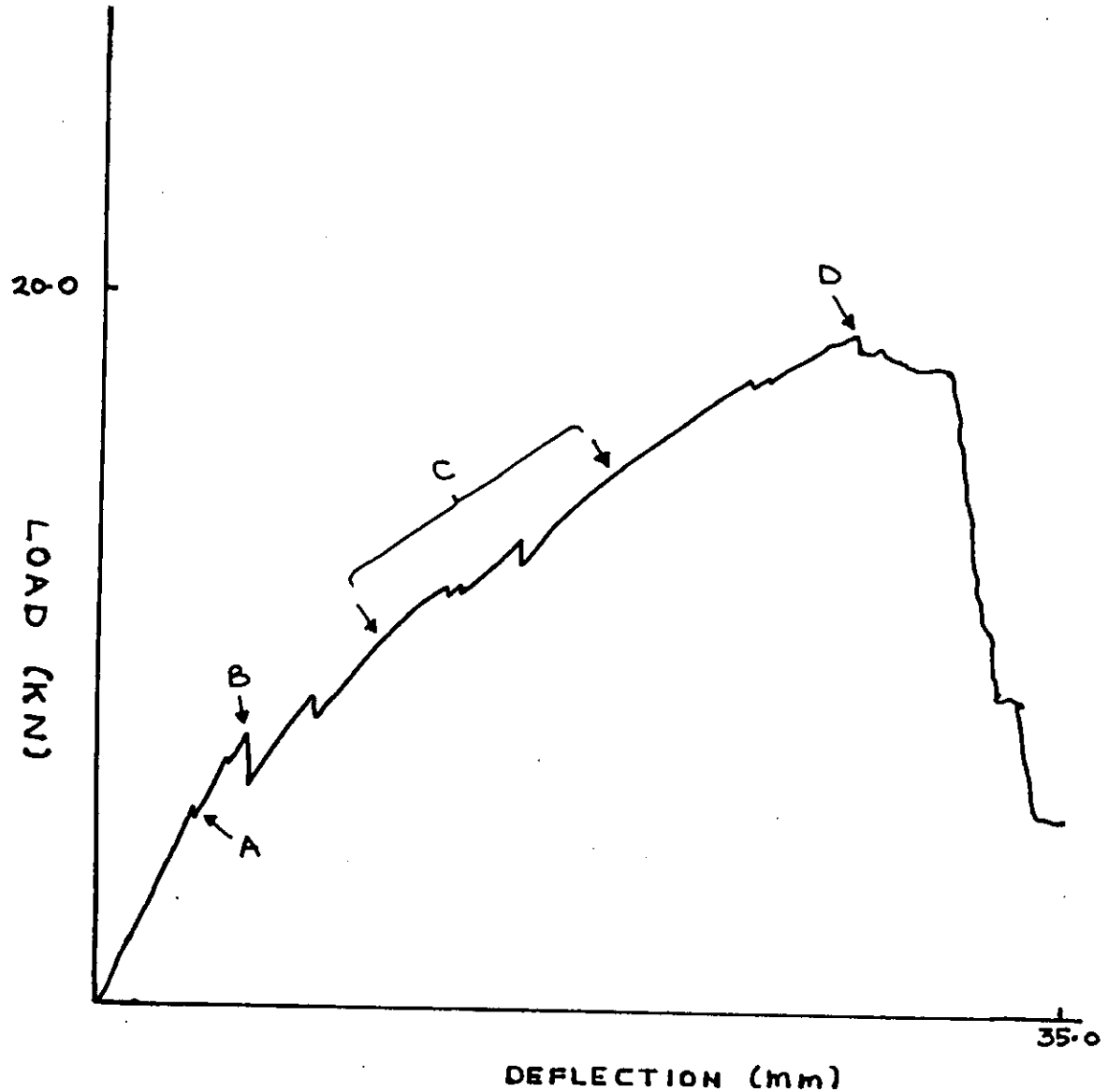

Figure 3.3 Experimental Load-Deflection Curve with Observed Failure Scenario.

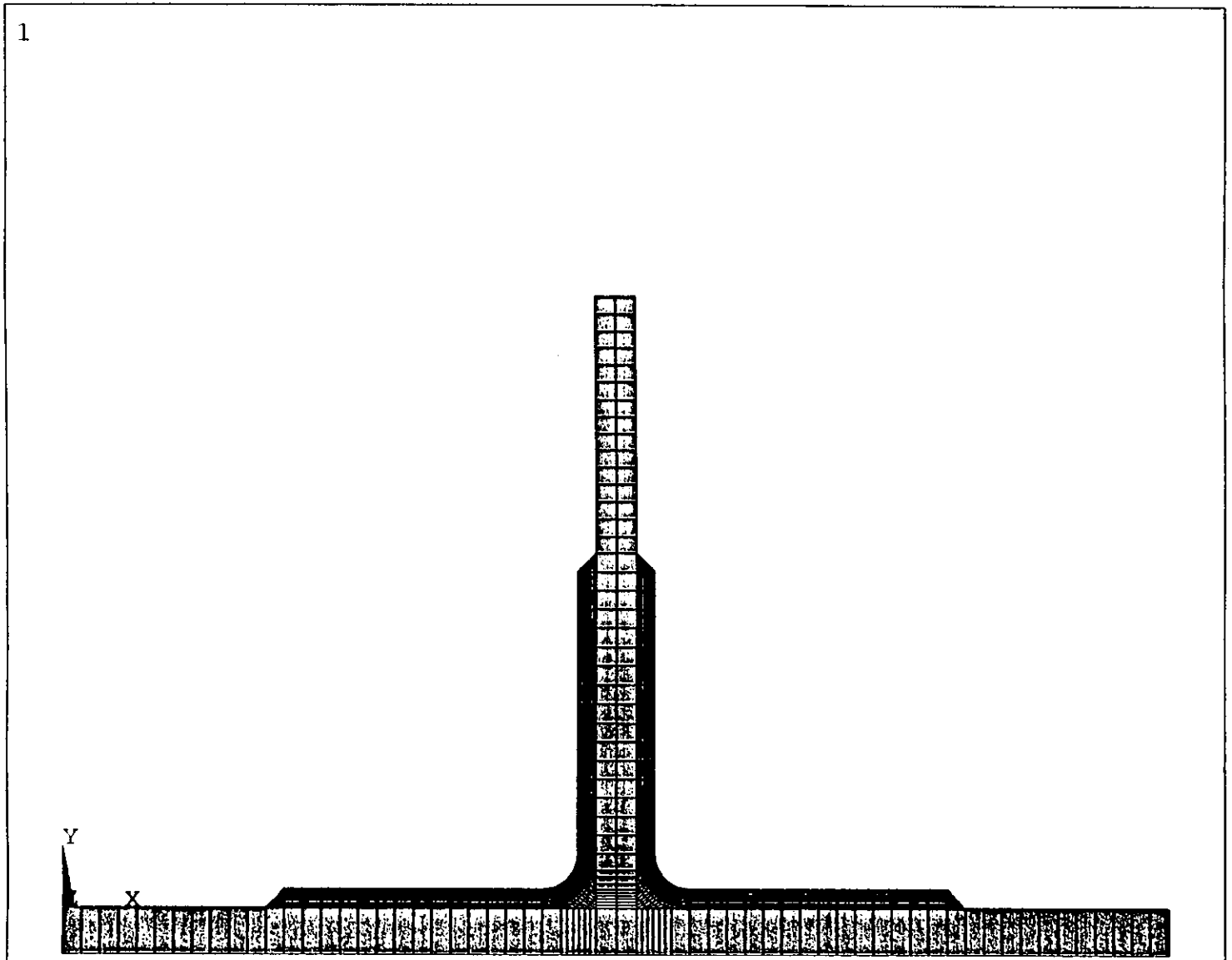

Figure 3.4 Finite Element Model of T-Joint.

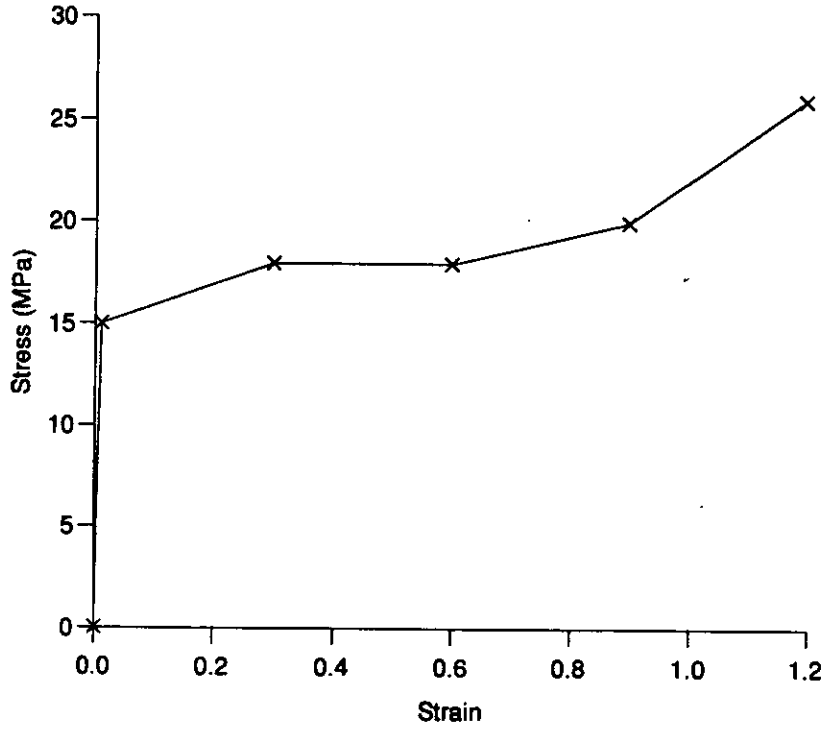

Figure 3 .5 Fillet Material assumed Stress/Strain Curve.

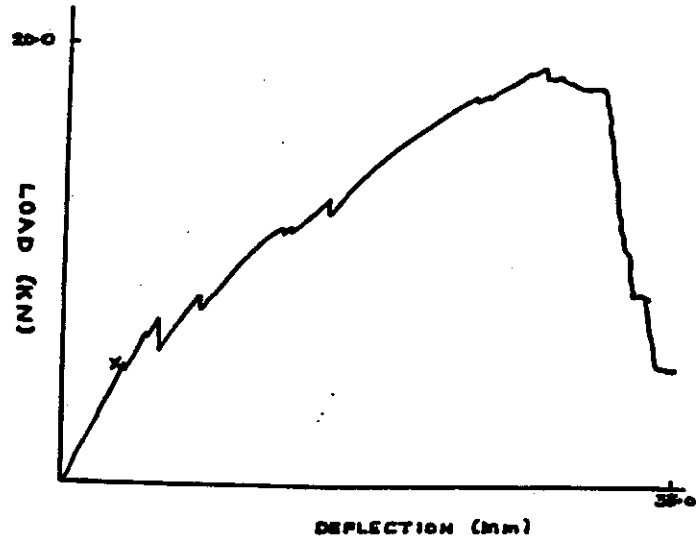

(a) Model 1.

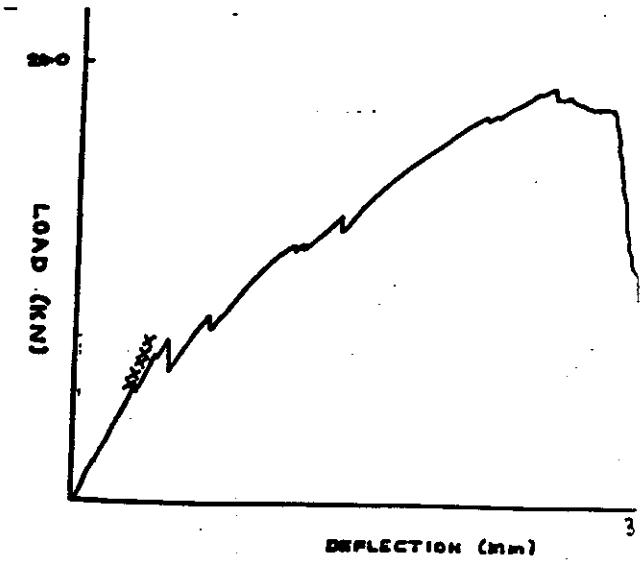

(b) Model 2.

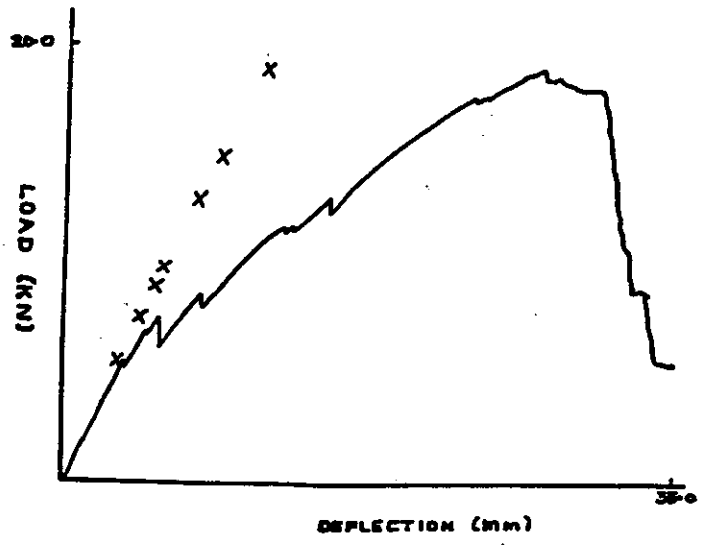

(c) Model 3.

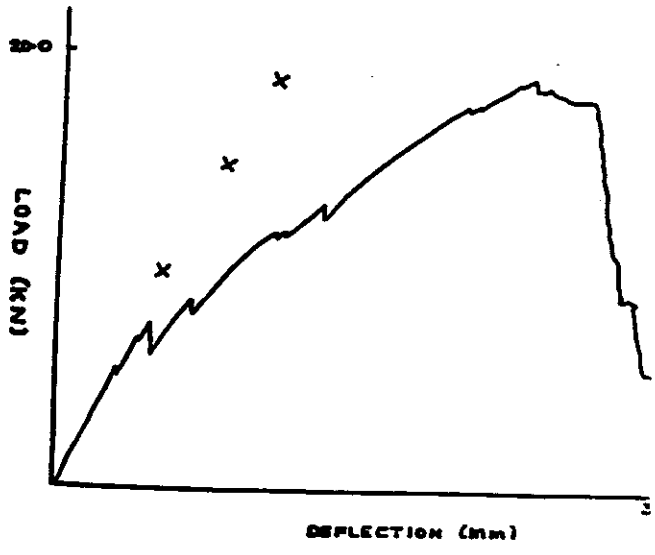

(d) Model 4.

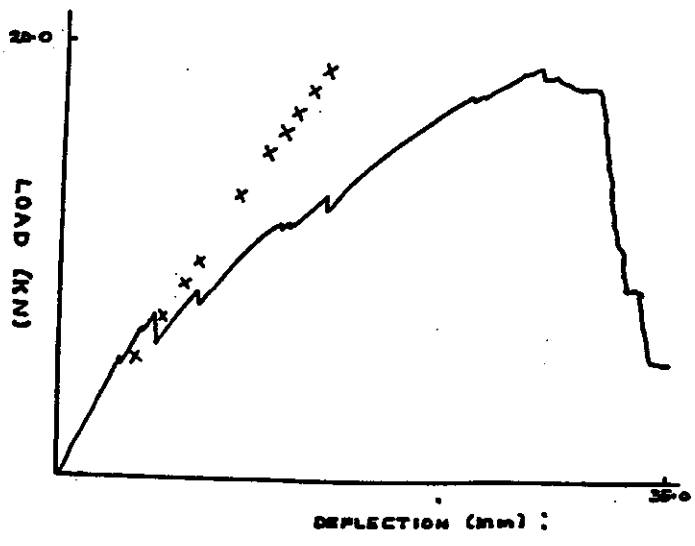

(e) Model 5.

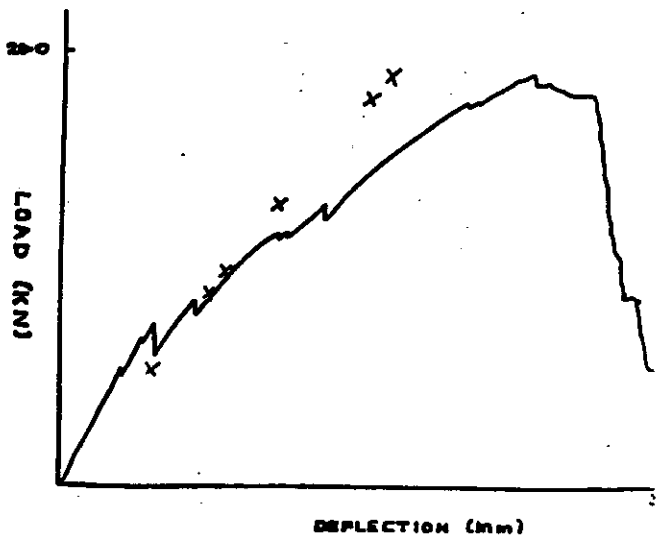

(f) Model 6.

Figure 3.6 Experimental and Finite Element Derived Load/Deflection Curves.

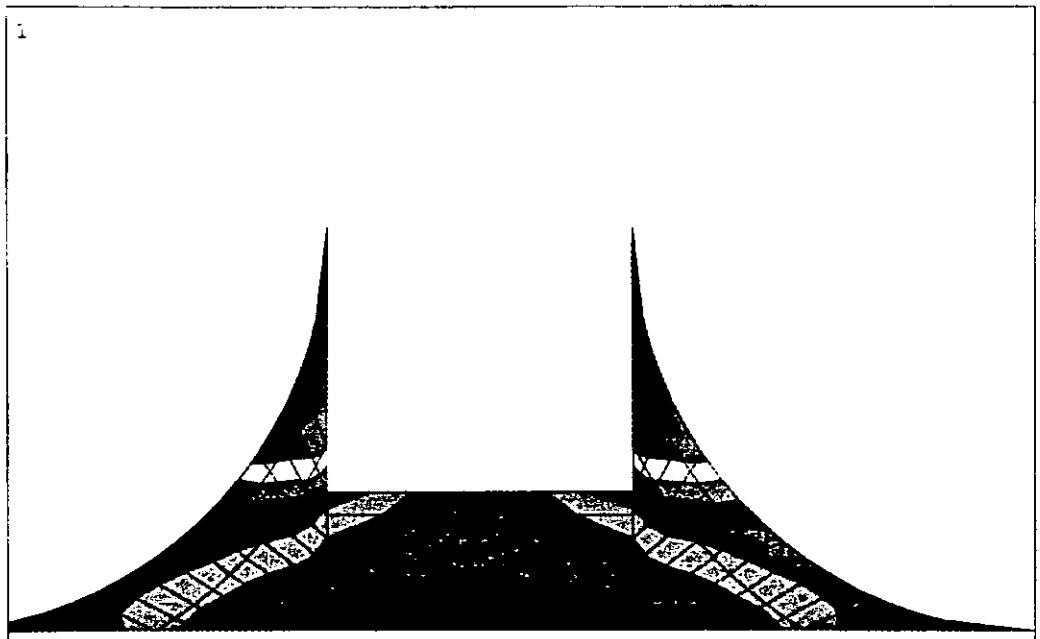

Figure 3.7(a) Model 1 : Typical Fillet Principal Stress Distribution.

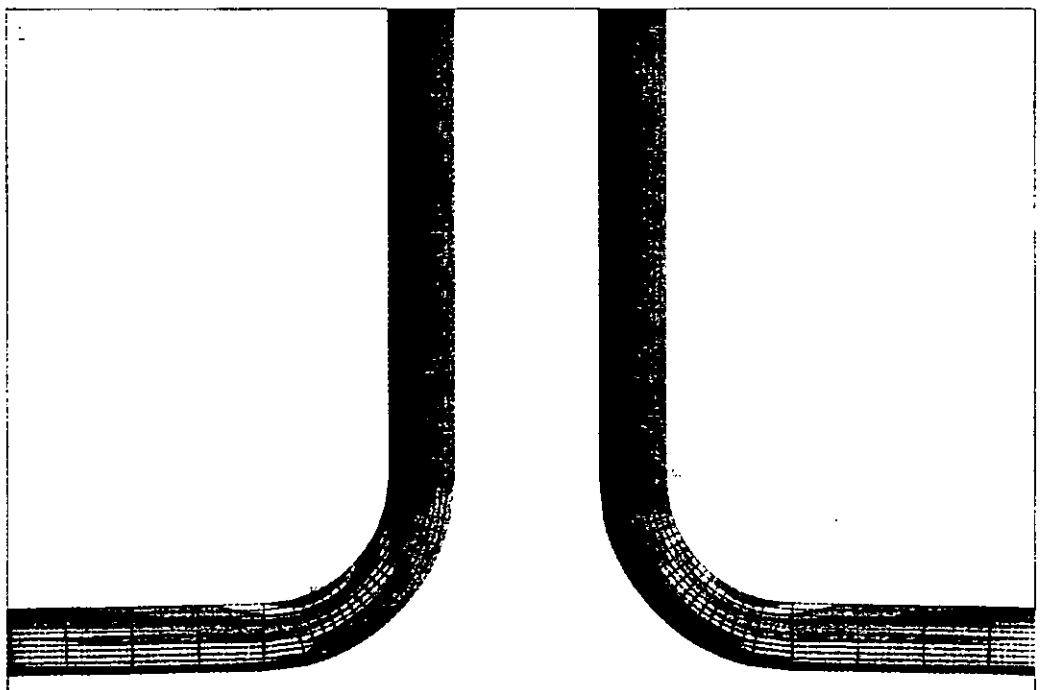

Figure 3.7(b) Model 1 : Typical Overlaminate In-Plane Stress Distribution.

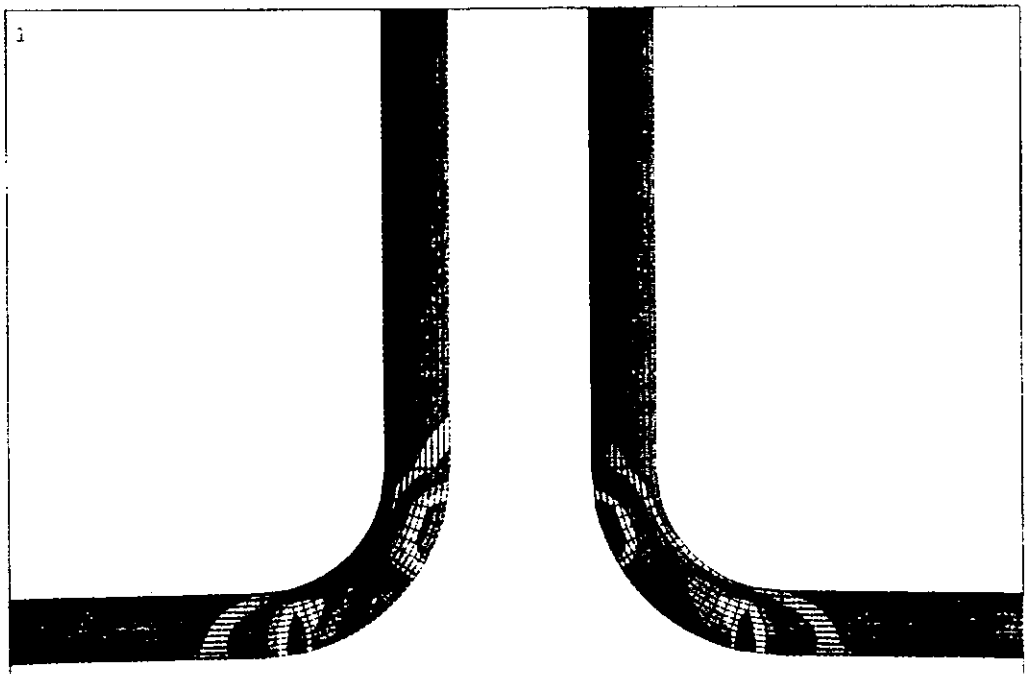

Figure 3.7(c) Model 1 : Typical Overlaminate Through-Thickness Stress Disribution.

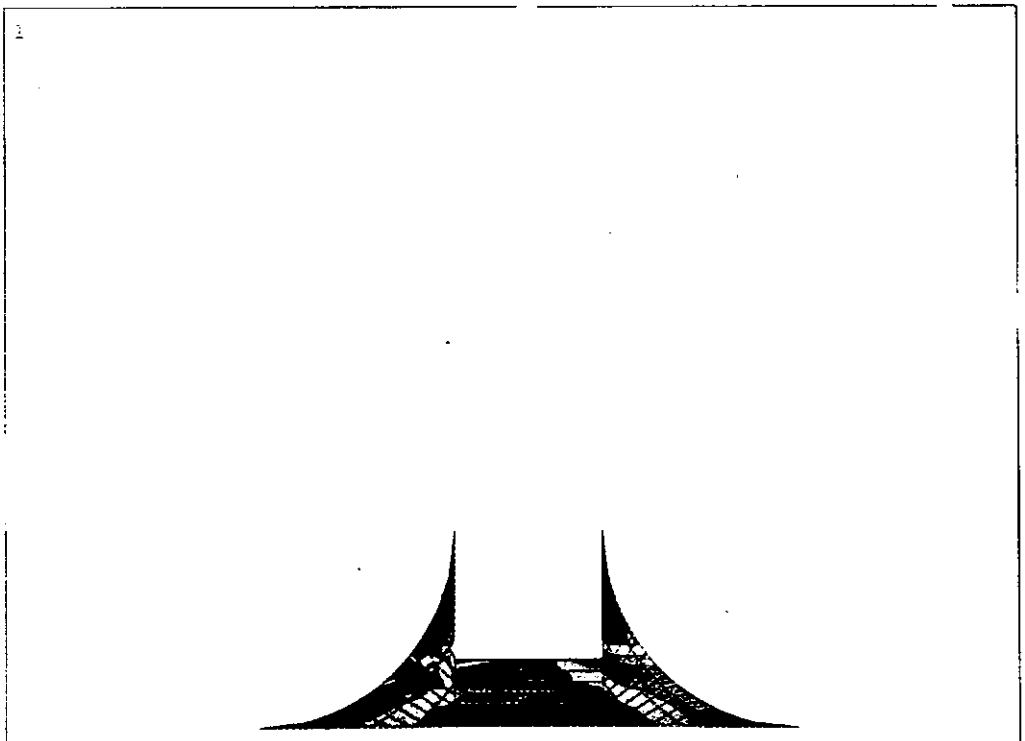

Figure 3.8(a) Model 2 : Typical Fillet Principal Stress Distribution.

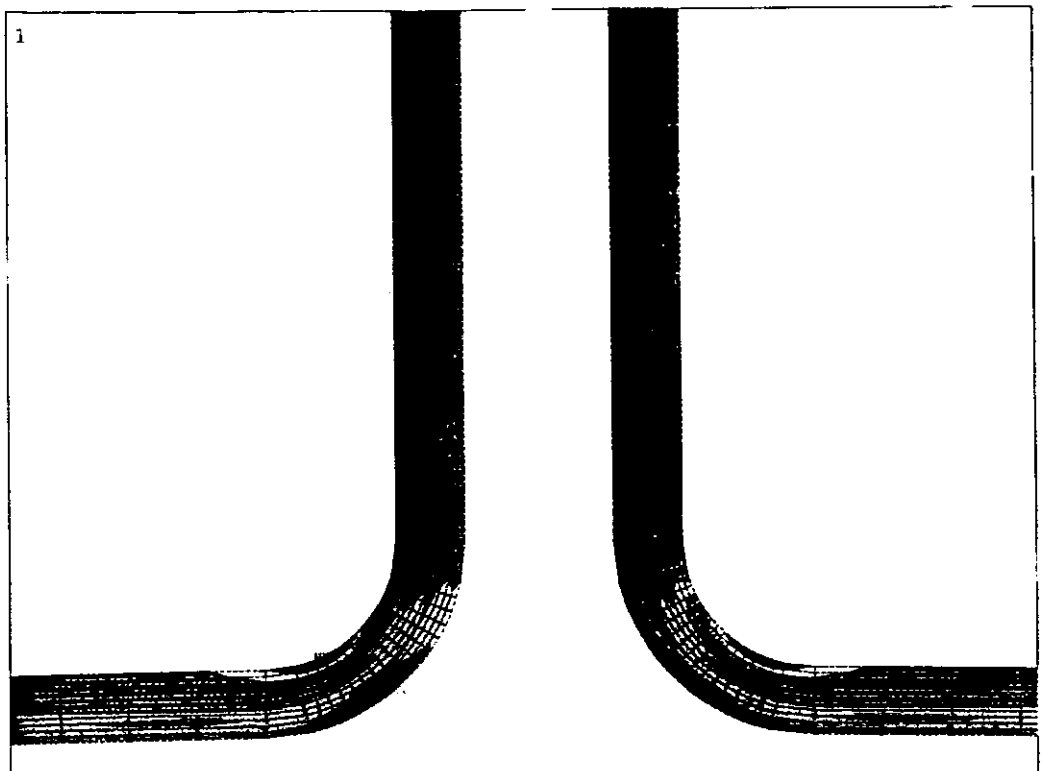

Figure 3.8(b) Model 2 : Typical Overlaminate In-Plane Stress Distribution.

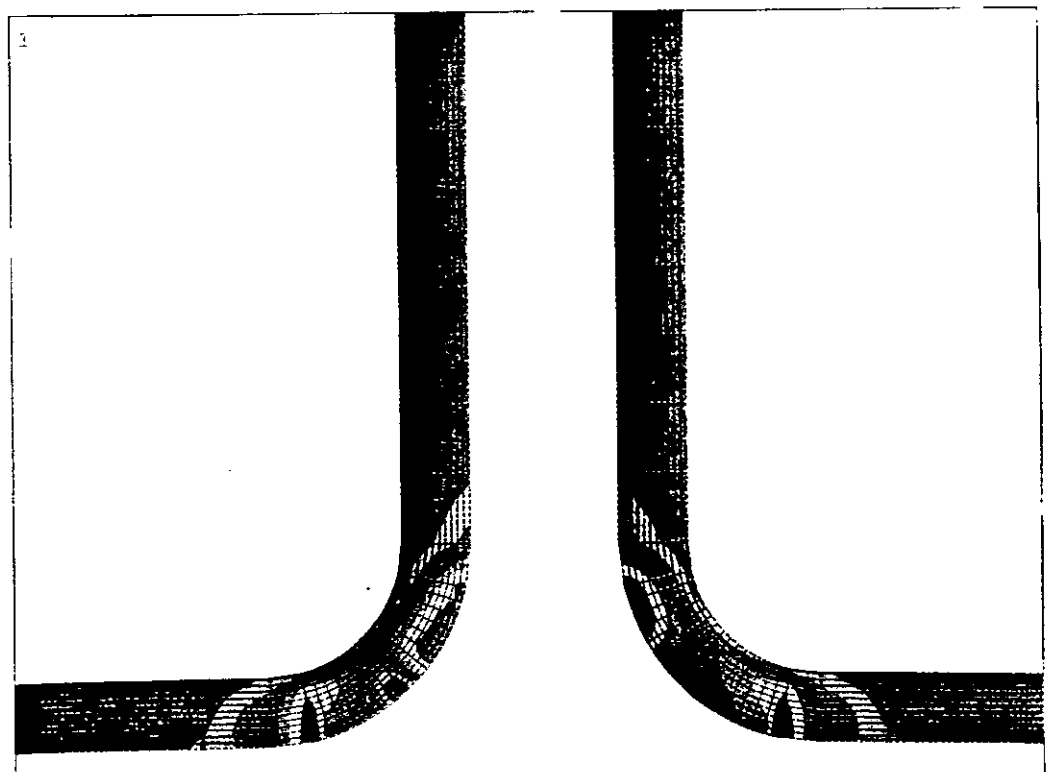

Figure 3.8(c) Model 2 : Typical Overlaminate Through-Thickness Stress Disribution.

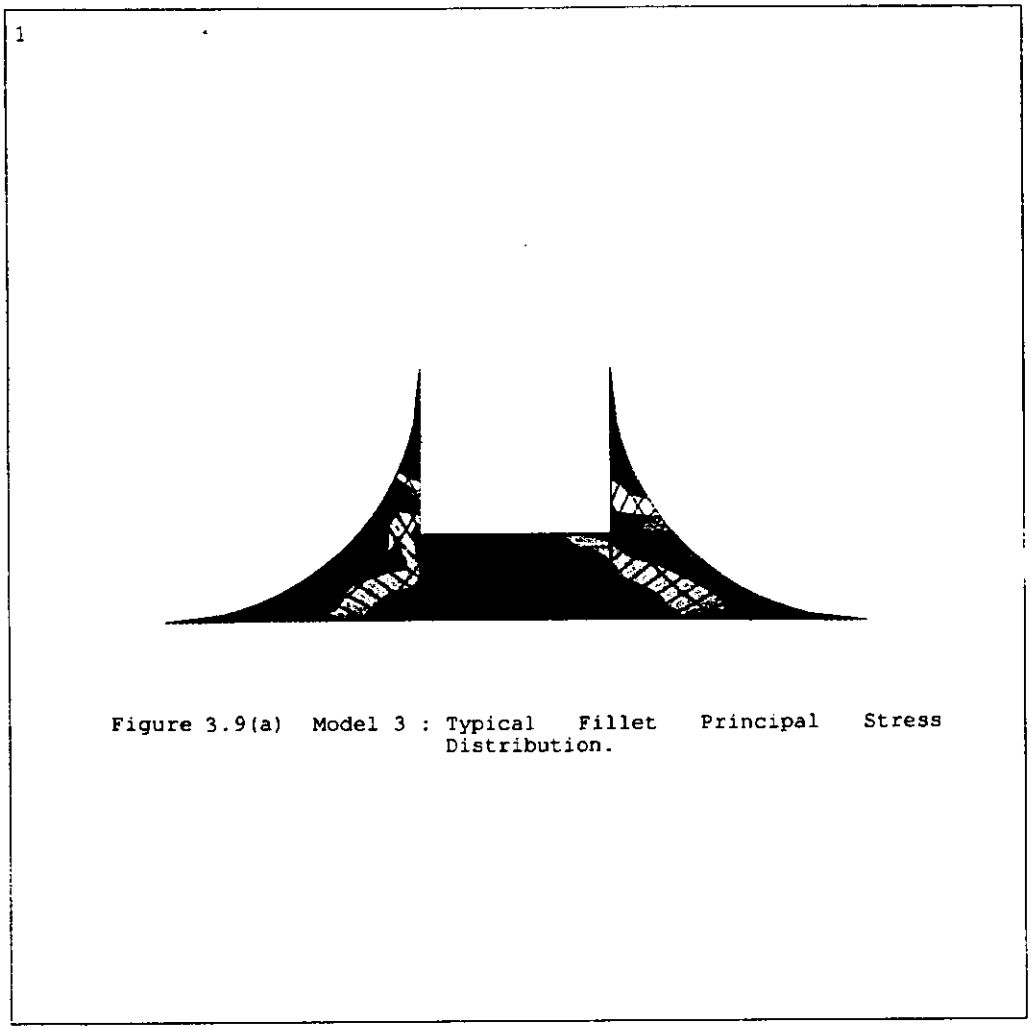

Figure 3.9(a) Model 3 : Typical Fillet Principal Stress Distribution.

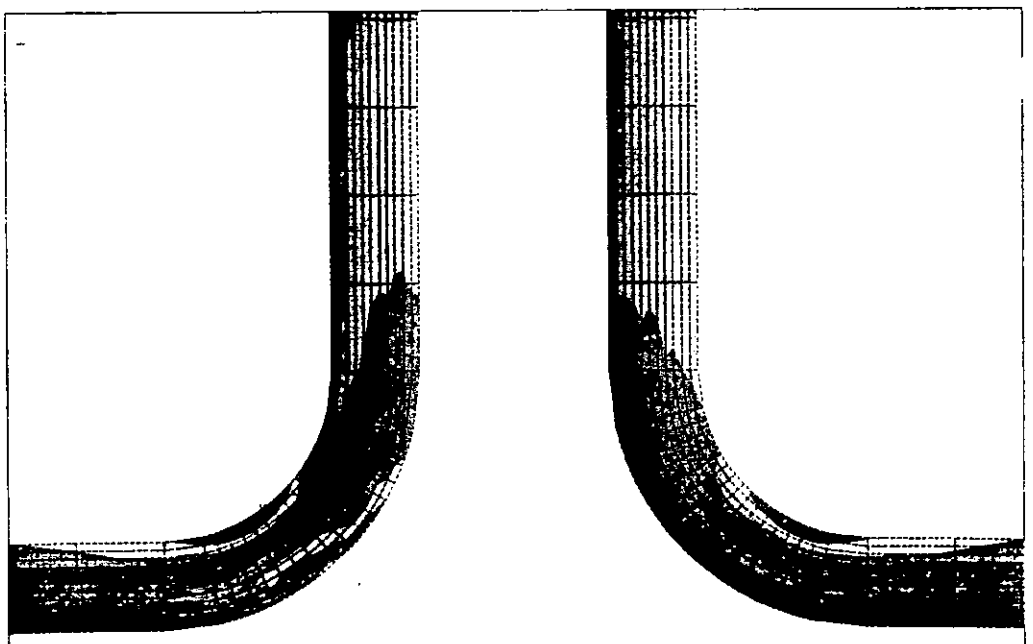

Figure 3.9(b) Model 3 : Typical Overlaminate In-Plane Stress Distribution.

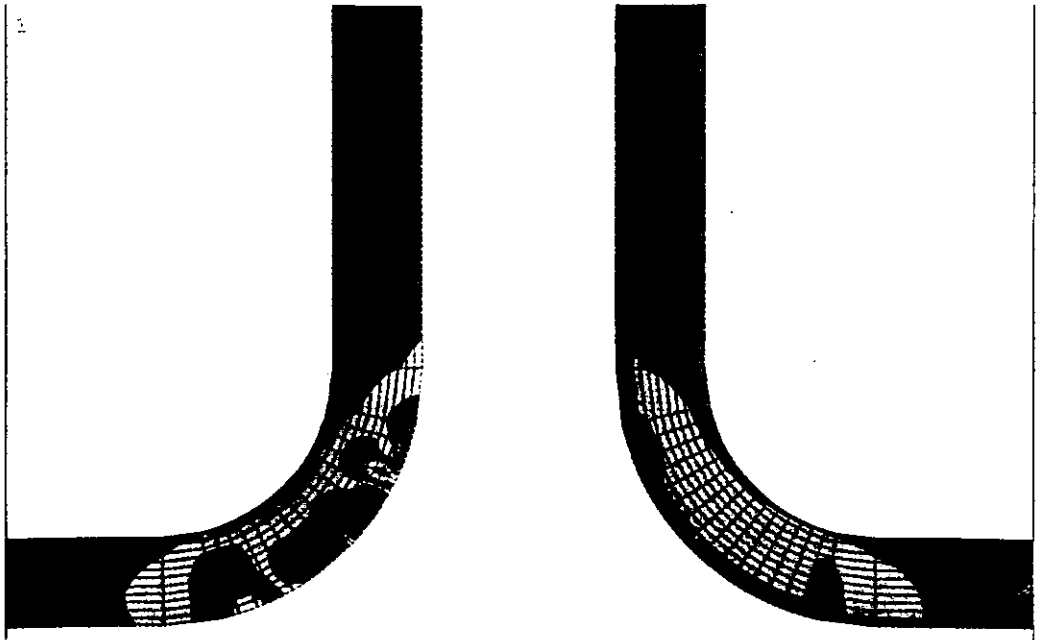

Figure 3.9(c) Model 3 : Typical Overlaminate Through-Thickness Stress Disribution.

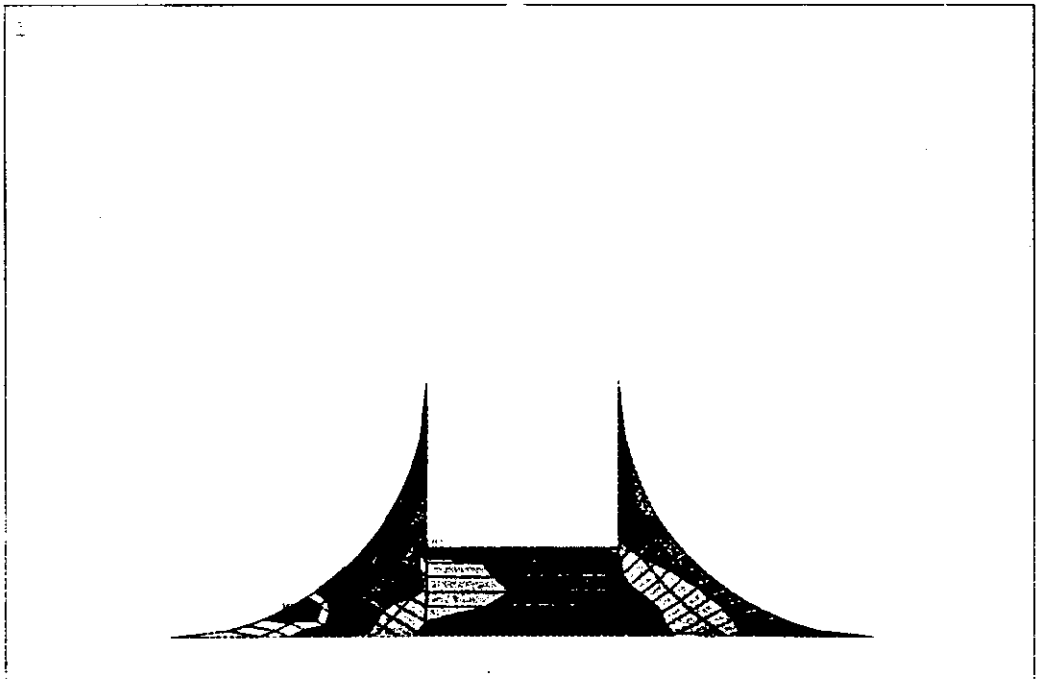

Figure 3.10(a) Model 4 : Typical Fillet Principal Stress Distribution.

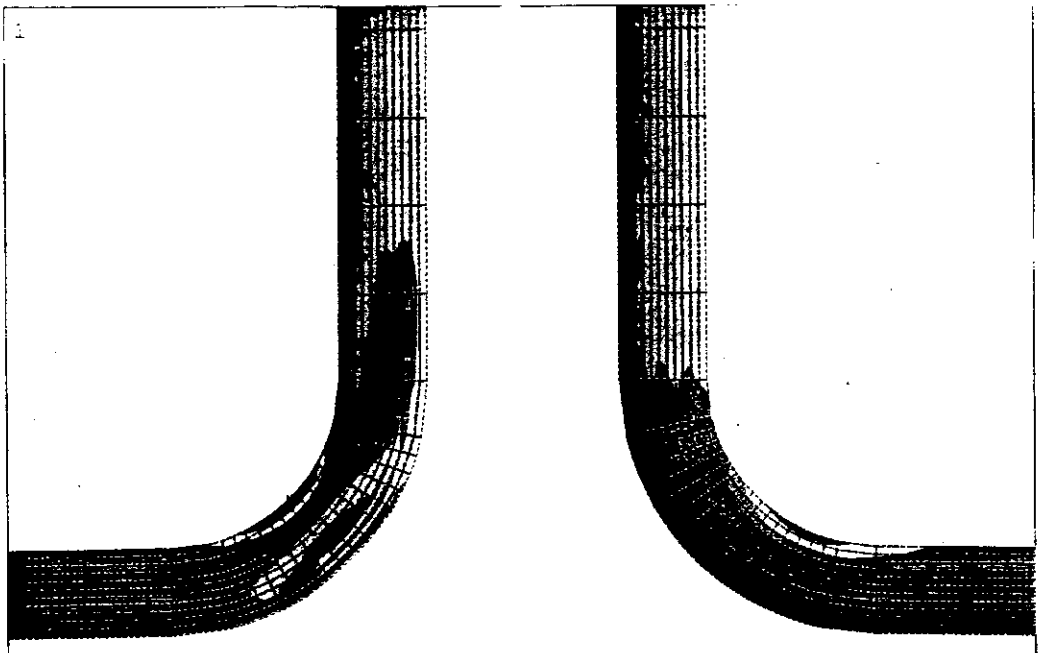

Figure 3.10(b) Model 4 : Typical Overlaminate In-Plane Stress Distribution.

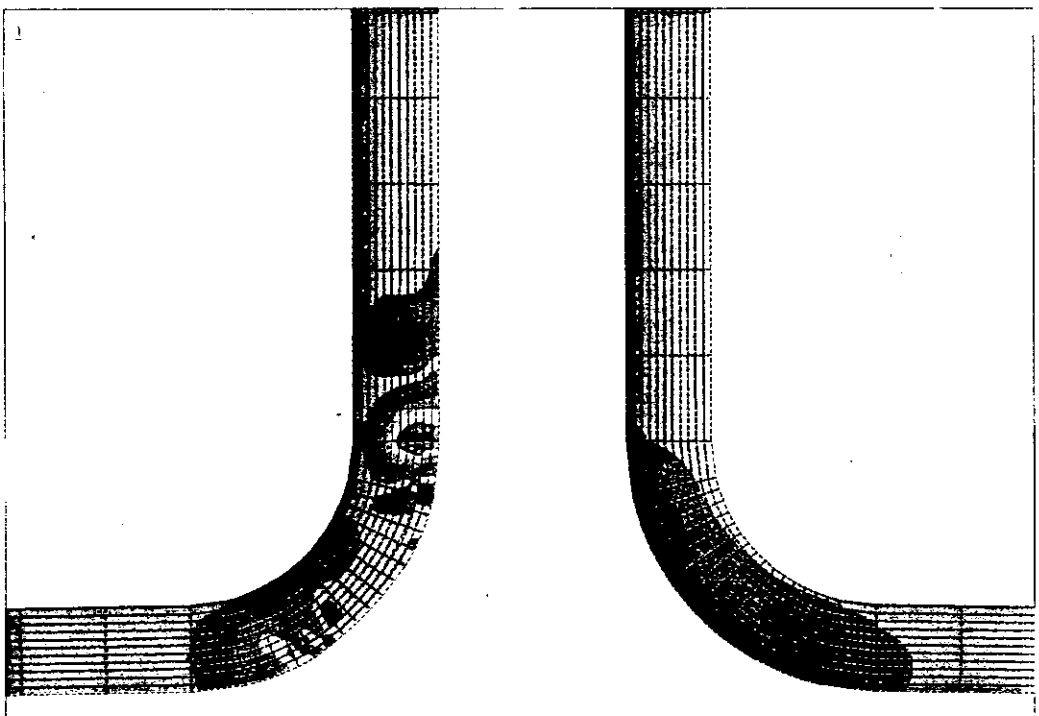

Figure 3.10(c) Model 4 : Typical Overlaminate Through-Thickness Stress Disribution.

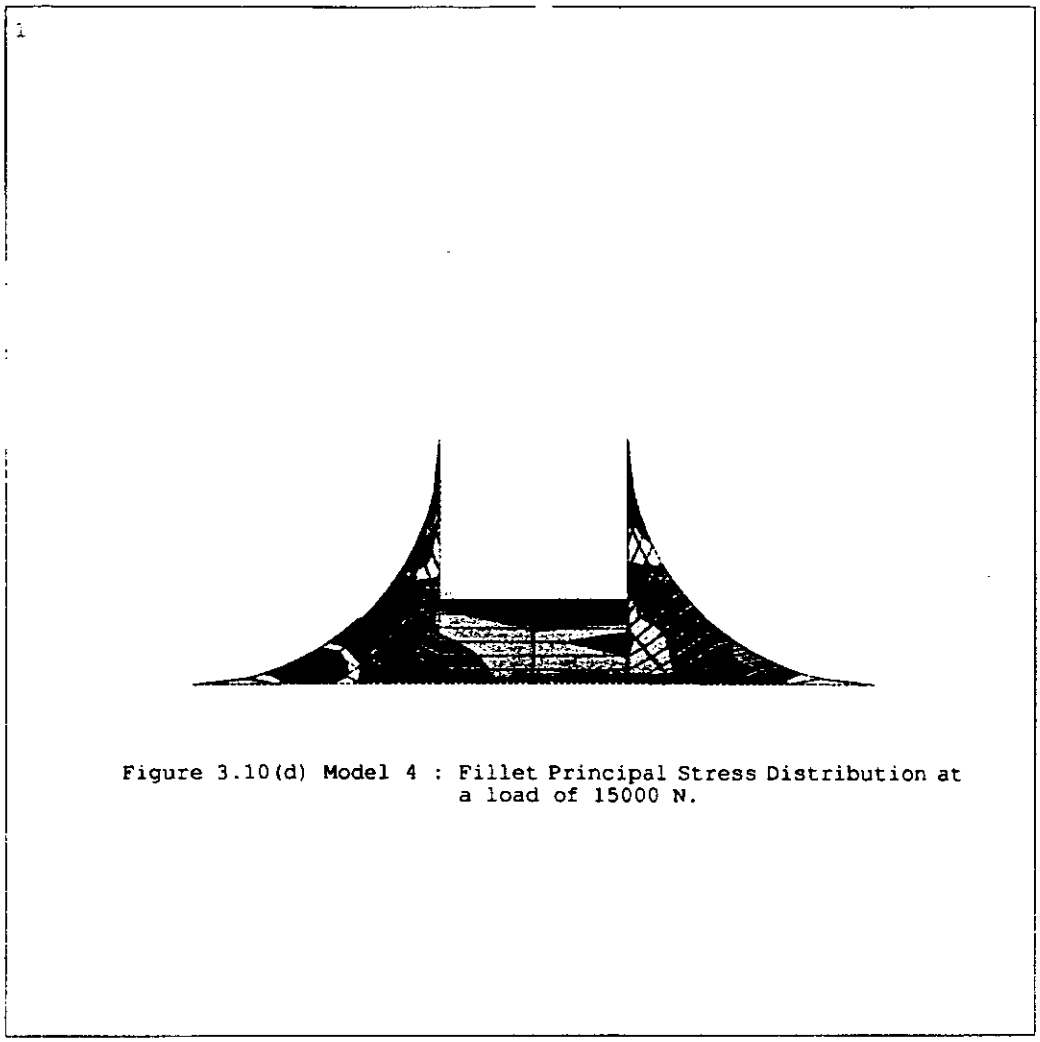

Figure 3.10(d) Model 4 : Fillet Principal Stress Distribution at a load of 15000 N.

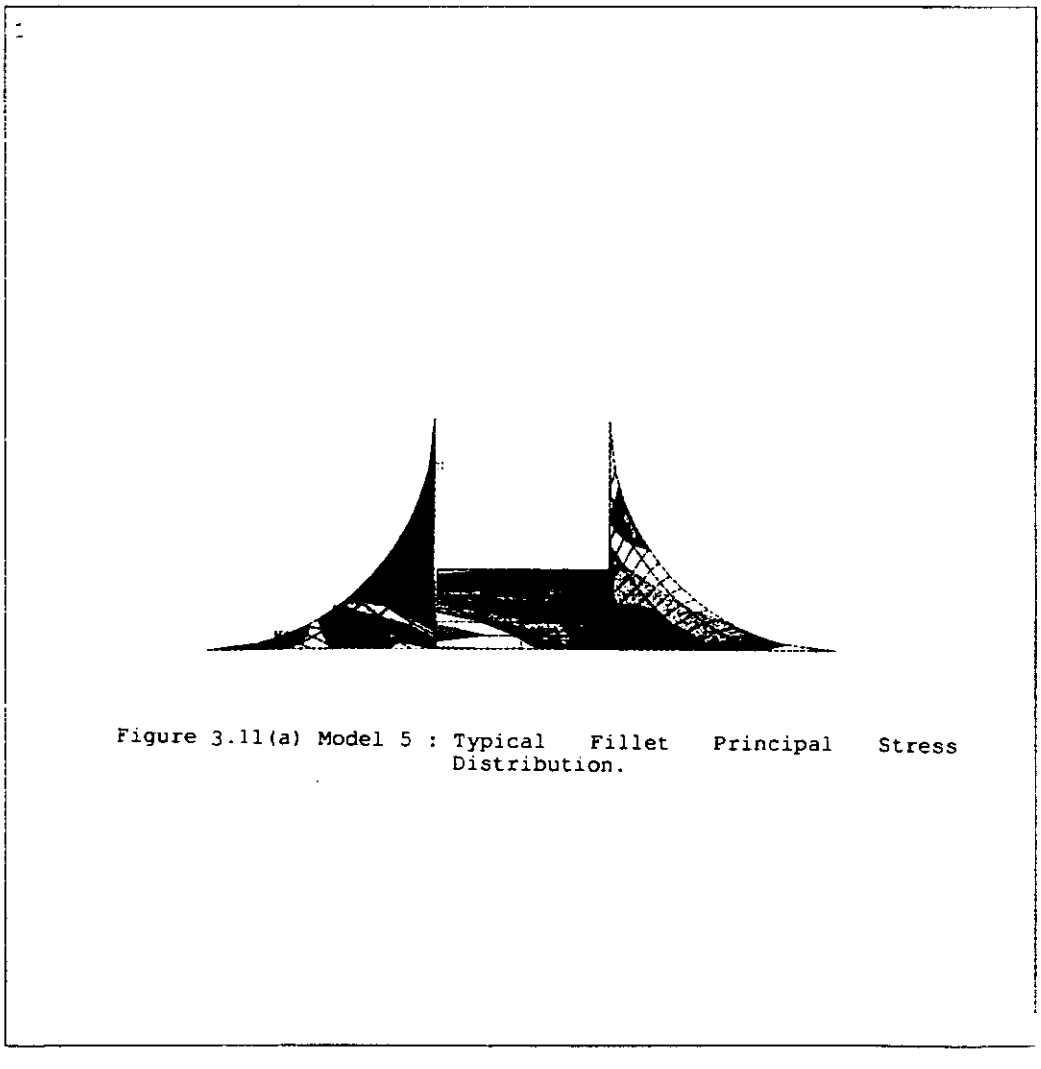

Figure 3.11(a) Model 5 : Typical Fillet Principal Stress Distribution.

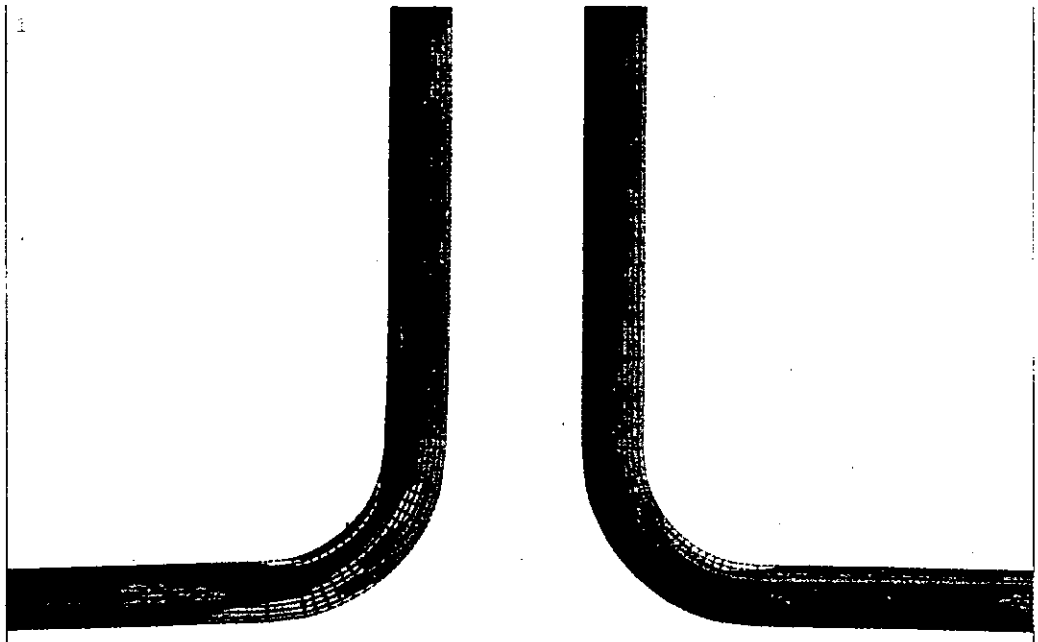

Figure 3.11(b) Model 5 : Typical Overlaminate In-Plane Stress Distribution.

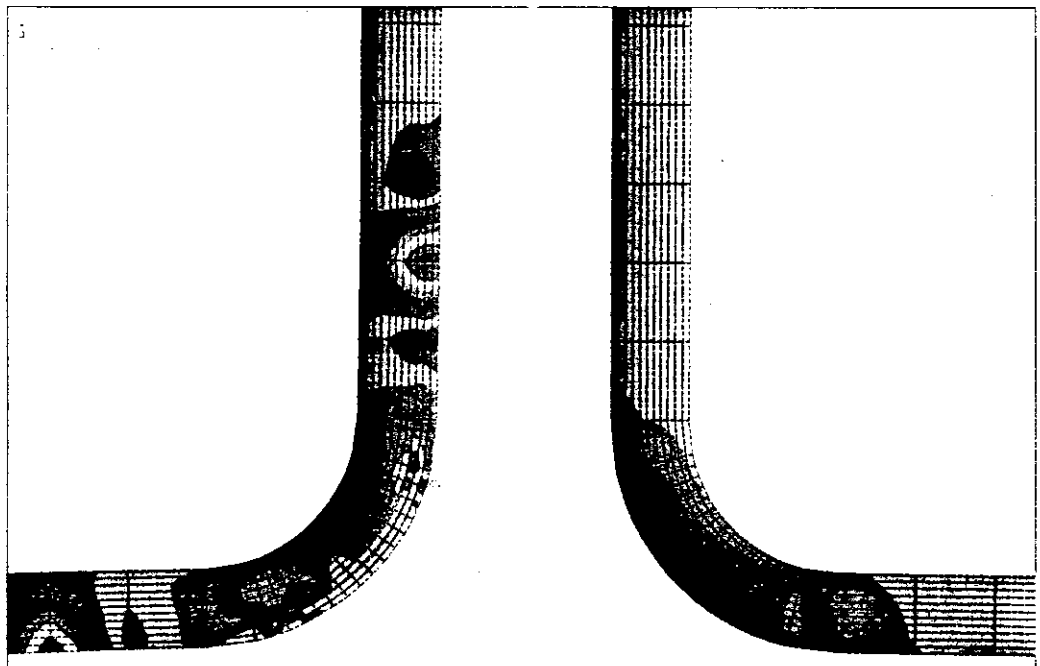

Figure 3.11(c) Model 5 : Typical Overlaminate Through-Thickness Stress Disribution.

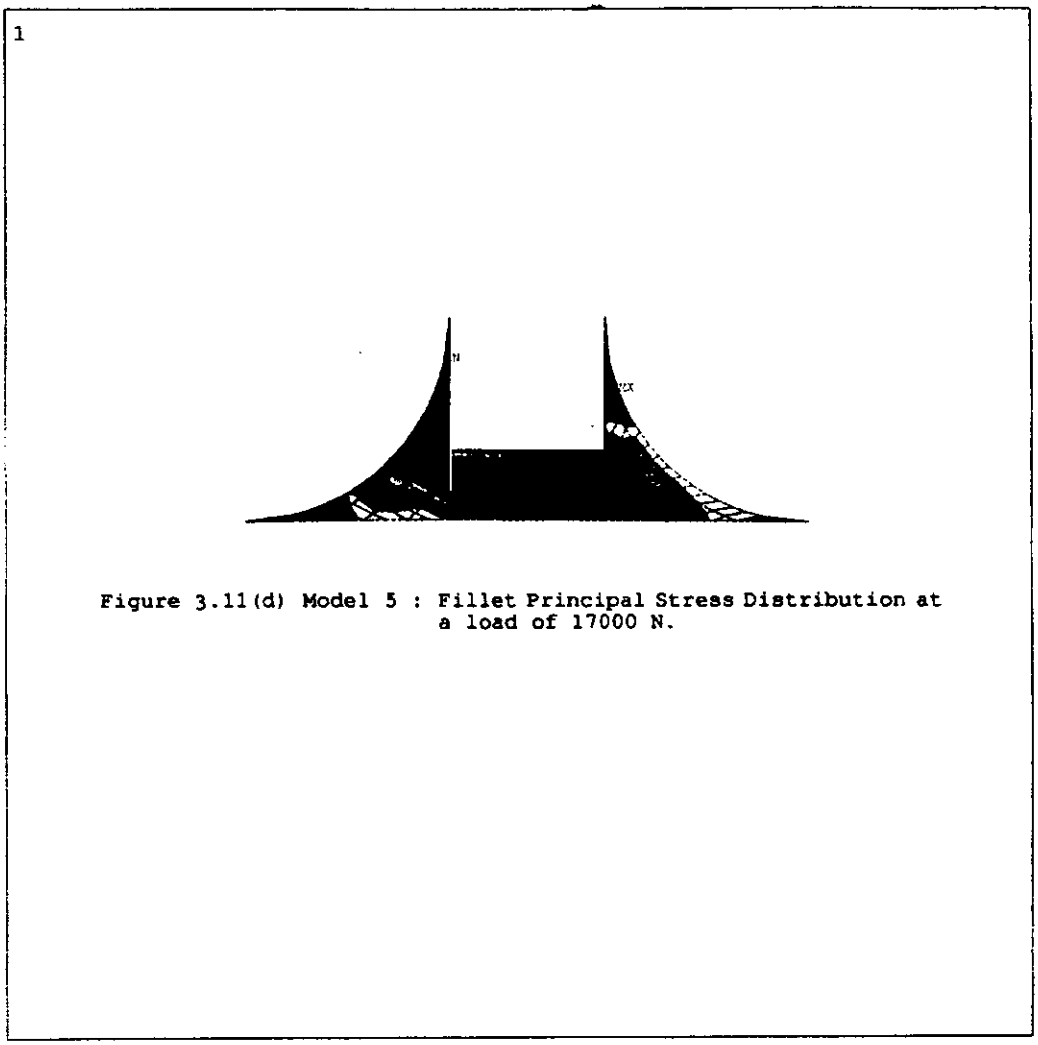

Figure 3.11(d) Model 5 : Fillet Principal Stress Distribution at a load of 17000 N.

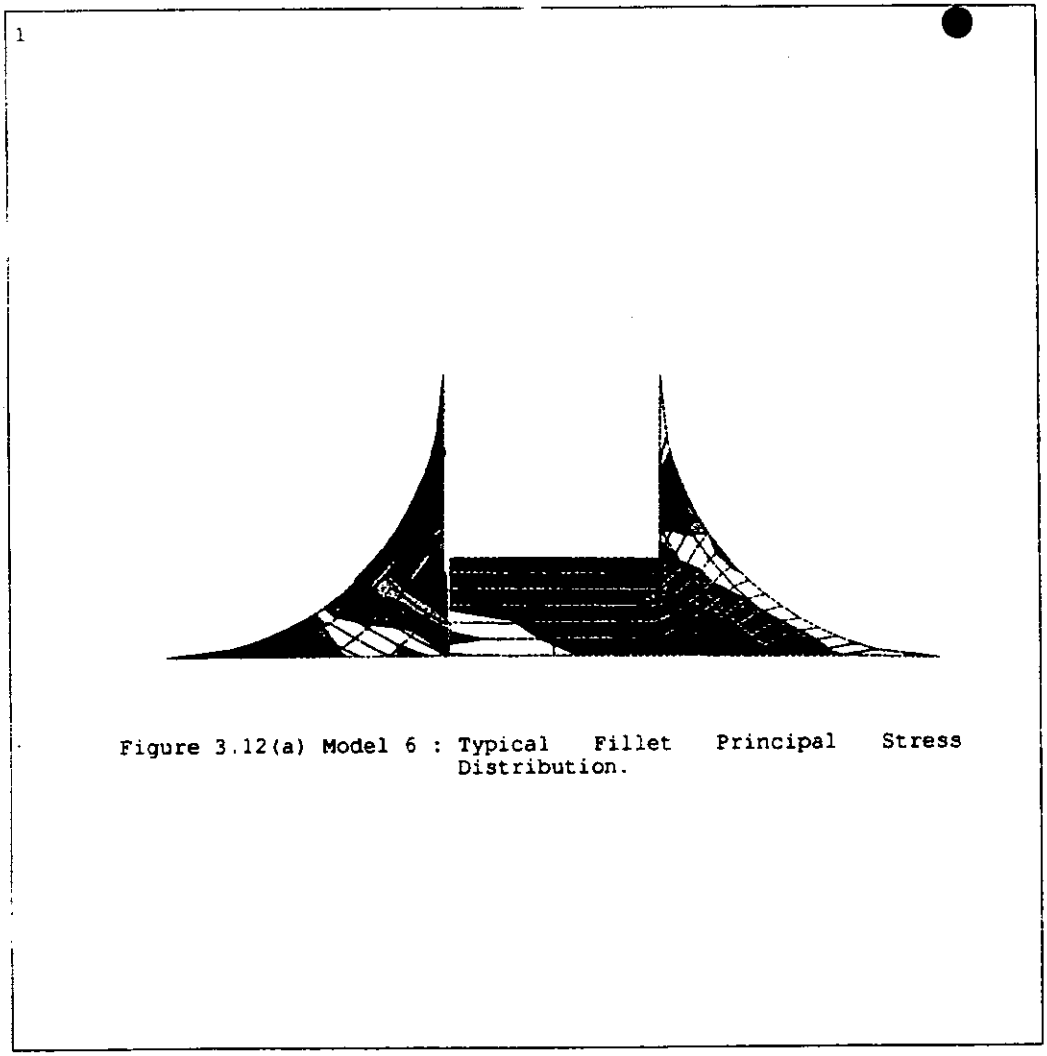

Figure 3.12(a) Model 6 : Typical Fillet Principal Stress Distribution.

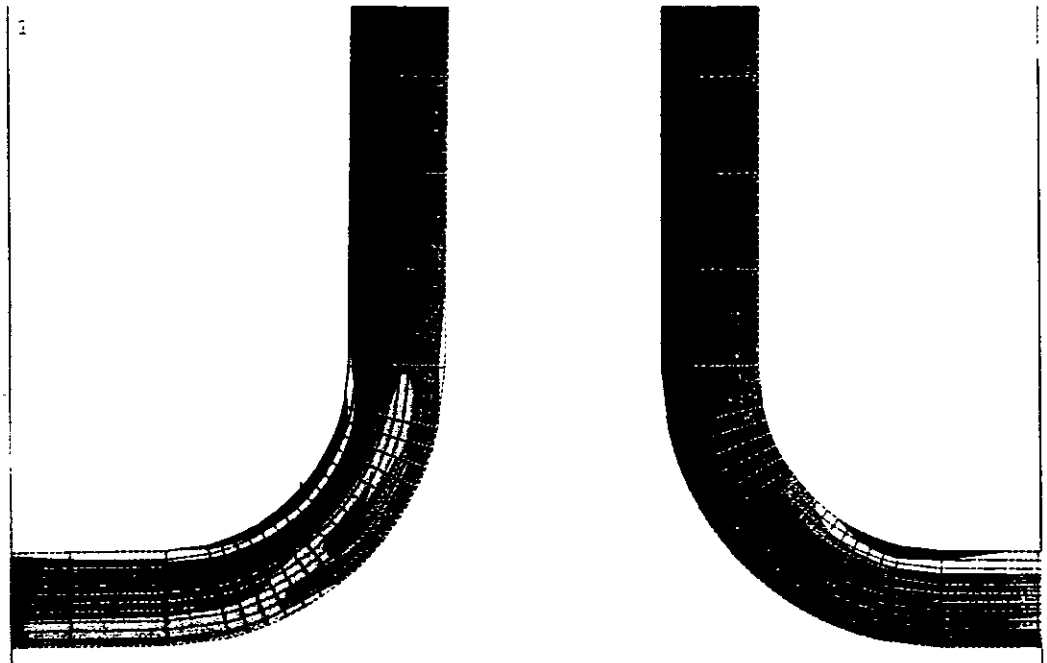

Figure 3.12(b) Model 6 : Typical Overlaminate In-Plane Stress Distribution.

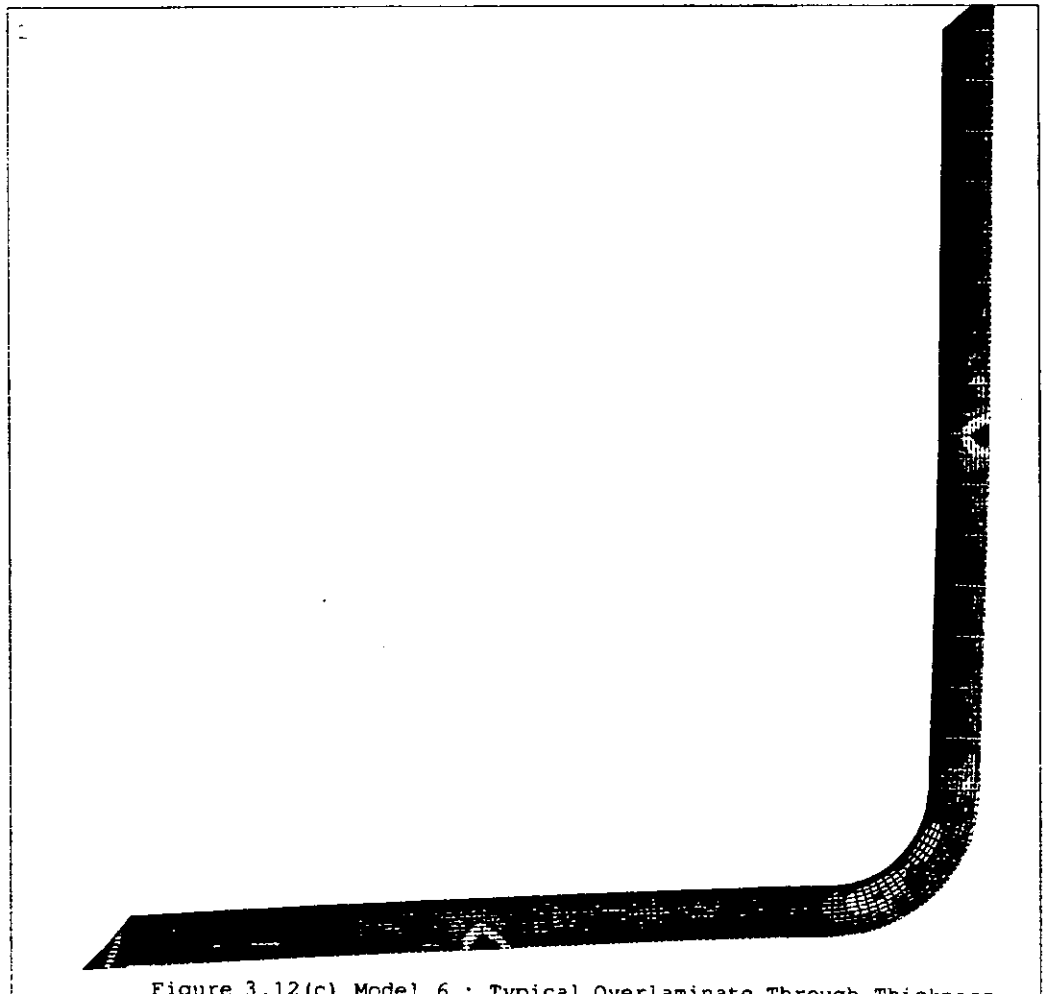

Figure 3.12(c) Model 6 : Typical Overlaminate Through-Thickness Stress Disribution.

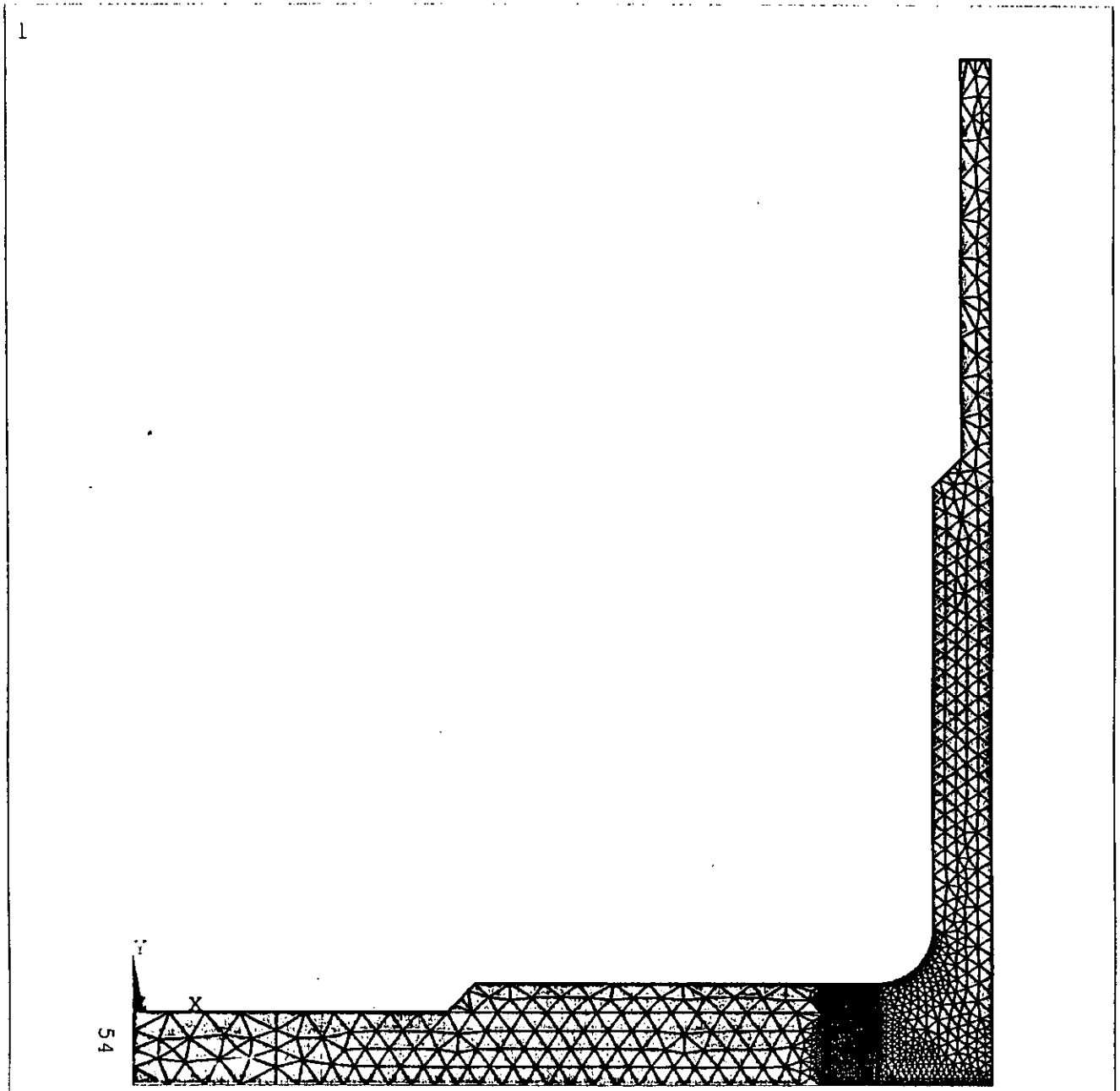

Figure 4.1 Finite Element Model generated using 2D plane strain elements.

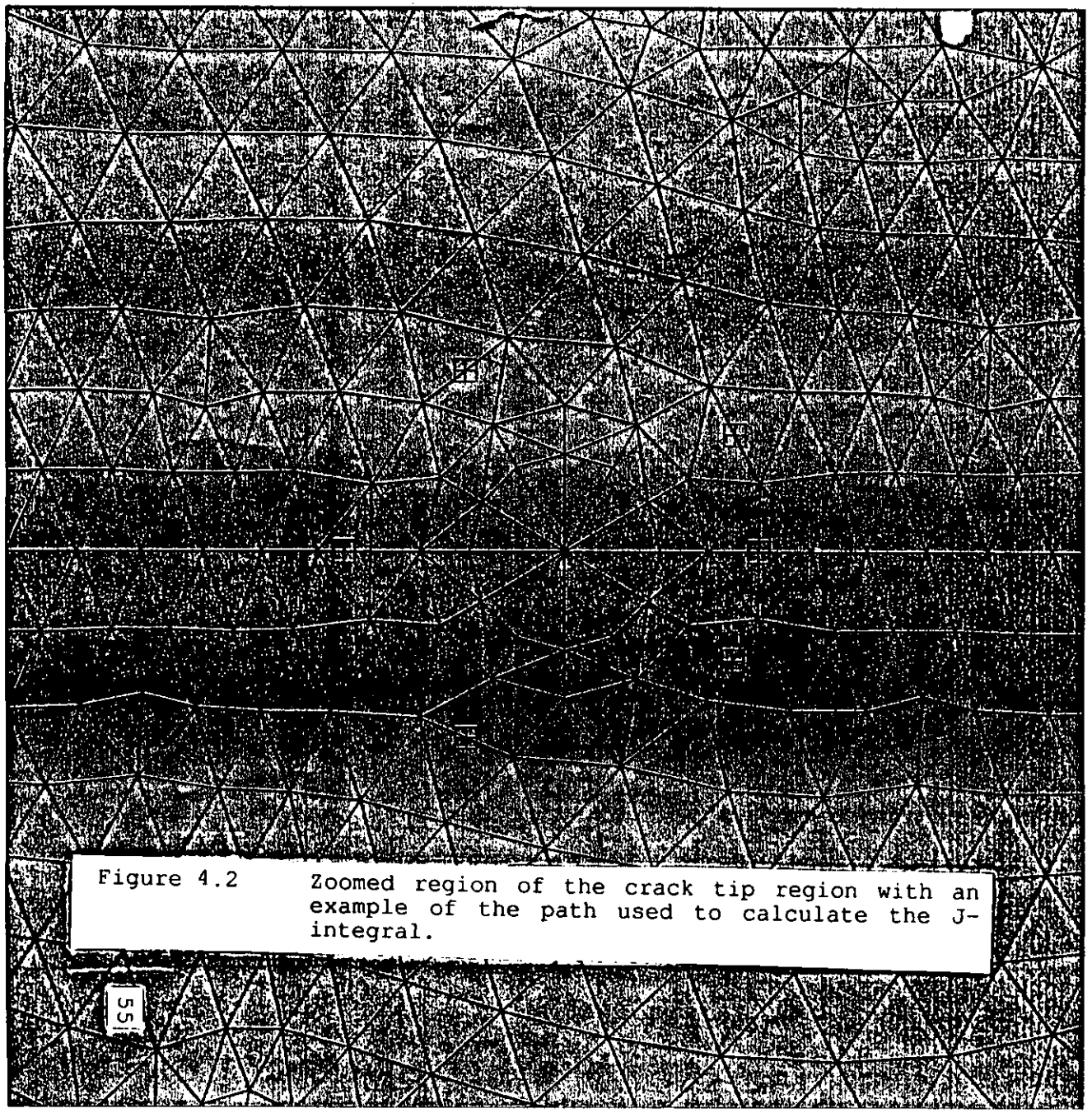

Figure 4.2 Zoomed region of the crack tip region with an example of the path used to calculate the J-integral.

TABLES.

Between ply numbers	Hand Lay-up Depth from outer surface (mm)	V.R.T. Depth from outer surface (mm)
1 - 2	0.8	0.53
2 - 3	1.7	1.06
3 - 4	2.4	1.59
4 - 5	3.6	2.12
5 - 6	4.2	-

Table 2.1. Delamination location for all beam specimens.

No. elements along defect region	Aspect ratio of elements in defect region	Critical Stress (MPa) analytical results	Critical Stress (MPa) experimental results	Critical Stress (MPa) F.E. results	Buckled Shape
4	10.0	100.7	71.28	148.64	typical
5	12.5	100.7	71.28	126.78	typical
6	15.0	100.7	71.28	76.473	non-typical
10	25.0	100.7	71.28	7.257	non-typical

Table 2.2 Effect of number of elements along defect region on Critical Buckling Stress and buckled shape. (Previous Analysis ref. [4]).

specimen type and modelling technique	distance below outer surface (mm)	delam. length (mm)	critical buckling stress (MPa)	buckled shape
V.R.T. (ANAL.)	0.53	60	8.01	-
V.R.T. (F.E 3D)	0.53	60	8.068	typical
V.R.T. (F.E 2D)	0.53	60	7.4420	typical

Table 2.3 Comparison of analytical and finite element derived values of critical buckling stress.

REFERENCE	LOAD (N)	DESCRIPTION
A	5500	Crack appeared in fillet
B	7500	First delamination appeared in overlaminate
C	10000-15000	Continuing delamination development
D	19000	Final failure: delaminations present between overlaminate/web interface and overlaminate/flange interface

Table 3.1. Experimentally observed T-Joint Failure Scenario.

MODEL/EXPT.	LOAD (N)	DEFLECTION (mm)	STIFFNESS (N/mm)
FULL 3D F.E. MODEL	5500	3.2128	1712
HALF 2D F.E. MODEL	5500	3.0447	1806
EXPERIMENT	5500	3.4375	1600

Table 3.2. Comparison of Preliminary Finite Element Results with Experimental values.

Material	**Region**	**Ex (MPa)**	**Ey (MPa)**	**nuxy**
Polyester/ Woven Roving	Web, Flange & over laminate	13060	7770	0.25
Polyester	over laminate	6890	7770	0.25
Crestomer	fillet	1500	1500	0.25

Table 3.3 Material Properties used in Finite Element Models.

MODEL	LOAD (N)	VERT. DEFL'N (mm)	HORIZ. DEFL'N (mm)	S1 max. (MPa)	SX max. (MPa)	SY max. (MPa)
undam.	5500	3.049	0.163	8.551	52.96	6.272

Table 3.4. Finite Element Results for Model 1.

where: S1 max. is the maximum principal stress in the fillet

SX max. is the maximum in-plane stress in the overlaminate

SY max. is the maximum through-thickness stress in the overlaminate

LOAD (N)	VERT. DEFL'N (mm)	HORIZ. DEFL'N (mm)	S1 max. (MPa)	E1 max.	SX max. (MPa)	SY max. (MPa)
5500	3.060	0.132	8.603	0.0054	54.00	6.33
6000	3.339	0.142	9.384	0.0059	58.90	6.90
6500	3.617	0.151	10.198	0.0064	63.79	7.47
7000	3.896	0.160	10.967	0.0069	68.68	8.04
7500	4.175	0.169	11.753	0.0074	73.58	8.61

Table 3.5. Finite Element Results for Model 2.

where: E1 max is the maximum principal strain in the fillet

The other notation is as before.

LOAD (N)	DEFL'N (mm)	HORIZ. DEFL'N (mm)	S1 max. (MPa)	E1 max.	SX max. (MPa)	SY max. (MPa)
5500	3.112	0.123	10.89	0.00674	59.09	21.62
7500	4.246	0.156	14.69	0.00913	80.46	29.43
9000	5.100	0.177	16.75	0.0129	96.44	35.74
10000	5.676	0.192	17.18	0.0192	107.06	39.88
13000	7.457	0.220	18.16	0.0411	139.31	50.99
15000	8.698	0.218	18.96	0.0572	161.49	59.37
19000	11.386	0.184	20.40	0.0976	211.18	75.00

Table 3.6. Finite Element Results for Model 3.

LOAD (N)	VERT. DEFL'N (mm)	HORIZ. DEFL'N (mm)	S1 max. (MPa)	E1 max.	SX max. (MPa)	SY max. (MPa)
10000	6.102	0.433	19.93	0.0196	119.8	25.25
15000	9.402	0.301	21.22	0.0466	180.42	39.397
19000	12.274	-0.03	21.41	0.0729	232.41	51.79

Table 3.7. Finite Element Results for Model 4.

LOAD (N)	VERT. DEFL'N (mm)	HORIZ. DEFL'N (mm)	S1 max. (MPa)	E1 max.	SX max. (MPa)	SY max. (MPa)
5500	4.256	1.931	6.982	0.00455	77.675	10.867
7500	5.798	2.595	10.544	0.00686	105.82	14.815
9000	6.953	3.079	11.379	0.00739	126.89	17.790
10000	7.722	3.395	12.257	0.00800	140.97	19.786
13000	10.065	4.265	16.304	0.0139	184.39	26.048
15000	11.667	4.738	17.174	0.0200	213.77	30.421
16000	12.492	4.912	16.870	0.023	228.35	32.664
17000	13.327	5.037	17.481	0.0258	242.49	34.907
18000	14.171	5.101	17.702	0.0312	256.03	37.143
19000	15.020	5.120	17.795	0.0395	268.99	39.354

Table 3.8. Finite Element Results for Model 5.

LOAD (N)	VERT. DEFL'N (mm)	HORIZ. DEFL'N (mm)	S1 max. (MPa)	E1 max.	SX max. (MPa)	SY max. (MPa)
5500	5.171	3.415	11.69	0.00736	47.62	5.657
9000	8.500	5.600	16.264	0.0193	79.618	9.349
10000	9.471	6.232	15.166	0.0254	89.33	10.472
13000	12.447	8.051	16.873	0.0473	119.31	13.91
15000	14.499	9.208	16.941	0.0656	140.27	16.273
18000	17.597	10.805	17.012	0.092	171.76	19.828
19000	18.635	11.287	17.057	0.101	182.24	21.01

Table 3.9. Finite Element Results for Model 6.

LOCATION IN GLOBAL COORDINATES	NODE	HORIZONTAL DISPLACEMENT (mm)	VERTICAL DISPLACEMENT (mm)
X = 252.03 mm Y = 0.0	TOP	-0.0200	2.3233
X = 252.03 mm Y = 0.0	BOTTOM	-0.0219	2.3217
X = 255.1 mm Y = 0.0	TOP	-0.0177	2.3361
X = 255.1 mm Y = 0.0	BOTTOM	-0.0202	2.3335

Table 4.1 Results of displacement check on selected nodes along the crack.

MODEL NO.	LOAD (N/mm)	CRACK LENGTH (mm)	J-integral (KJ/m^2)
A	27.5	10.0	0.0124 (Γ_1)
B	27.5	10.0	0.0131 (Γ_2)
C	27.5	10.0	0.0089 (Γ_1)

Table 4.2 Finite Element Generated values of the J-integral